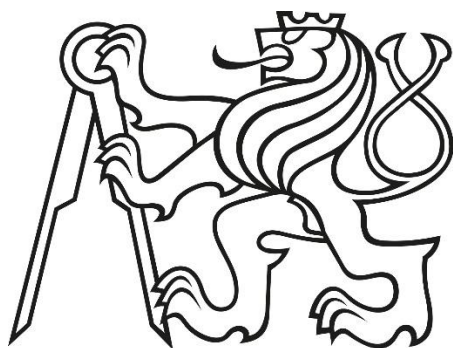


CZECH TECHNICAL UNIVERSITY IN PRAGUE

Faculty of Electrical Engineering
Department of Electromagnetic Field



Calibrator of xCW Radars

Diploma Thesis

Author:

Ing. Andrej Židkov

Supervisor:

Doc. Ing. Přemysl Hudec, CSc.

Prague, 2017

I. OSOBNÍ A STUDIJNÍ ÚDAJE

Příjmení: **Židkov** Jméno: **Andrej** Osobní číslo: **453177**
Fakulta/ústav: **Fakulta elektrotechnická**
Zadávající katedra/ústav: **Katedra elektromagnetického pole**
Studijní program: **Komunikace, multimédia a elektronika**
Studijní obor: **Bezdrátové komunikace**

II. ÚDAJE K DIPLOMOVÉ PRÁCI

Název diplomové práce:

Kalibrátor xCW radarů

Název diplomové práce anglicky:

Calibrator of xCW Radars

Pokyny pro vypracování:

Seznamte se způsoby realizace kalibrátorů radarů typu xCW (CW, FMCW, PNCW...). Navrhněte a realizujte zařízení schopné simulovat letící cíl pro radar typu PNCW, a to s následujícími hlavními parametry:

- o Střední frekvence 11 GHz;
- o Šířka pásma min. 1 GHz;
- o Vzdálenost cíle - je dána polohou kalibrátoru, může být konstantní;
- o Simulovaná rychlost cíle - , nastavitelná, min. 20m/s;
- o Simulované RCS - nastavitelné, min. 10-3 m²;
- o Řízení - pomocí mikropočítače, jednoduché klávesnice a zobrazovací jednotky.

Vlastnosti realizovaného zařízení ověřte na CW radaru 11 GHz.

Seznam doporučené literatury:

1. Li. R. Ch.: RF Circuit Design, John Wiley 2009.

Jméno a pracoviště vedoucí(ho) diplomové práce:

doc. Ing. Přemysl Hudec CSc., katedra elektromagnetického pole FEL

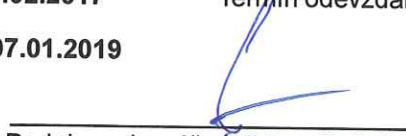
Jméno a pracoviště druhé(ho) vedoucí(ho) nebo konzultanta(ky) diplomové práce:

Datum zadání diplomové práce: **21.02.2017**

Termín odevzdání diplomové práce: _____

Platnost zadání diplomové práce: **07.01.2019**


Podpis vedoucí(ho) práce

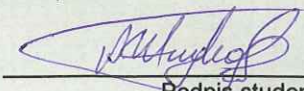

Podpis vedoucí(ho) ústavu/katedry


Podpis děkana(ky)

III. PŘEVZETÍ ZADÁNÍ

Diplomant bere na vědomí, že je povinen vypracovat diplomovou práci samostatně, bez cizí pomoci, s výjimkou poskytnutých konzultací. Seznam použité literatury, jiných pramenů a jmen konzultantů je třeba uvést v diplomové práci.

1.3.2017
Datum převzetí zadání


Podpis studenta

Abstract

Calibrator of xCW radars

This work is dedicated to design, realization, measurements and experimental verification of CW radar calibrator operating at 11 GHz frequency band. Theoretical background and principles of CW radars are given in the first two chapters of the thesis. Practical realization, as well as concepts of the calibrator for such type of the radars based on MMIC are explained in the third and in the fourth chapters. Measurement results and experimental testing are presented in the fifth chapter.

Keywords: radar calibration, CW Doppler radar.

Abstrakt

Kalibrátor xCW radarů

Tato práce se zabývá návrhem, realizací a experimentálním ověřením kalibrátoru dopplerovských radarů pracujících v pasmu 11 GHz. Teoretický základy a principy dopplerovských radarů jsou uvedeny v prvních dvou kapitolách práce. Praktická realizace a koncepty kalibrátoru pro tento typ radarů založených na MMIC jsou vysvětleny ve třetí a čtvrté kapitole. Výsledky měření a experimentální testování jsou uvedeny v páté kapitole.

Klíčová slova: kalibrace radarů, dopplerovské radary.

Acknowledgement

I would like to thank my supervisor Doc. Ing. Přemysl Hudec and Ing. Petr Ouredník for their useful advices, consultations and help during the work on this diploma thesis. I also would like to thank my colleagues Jan Zikmund and Josef Bartl for their support and valuable remarks.

Proclamation

I declare that this diploma thesis was written myself independently and only references stated herein were used according to “Methodical instruction about complying ethical principles during elaborating university thesis”. I have no objections against lending, publishing and any other utilization as long as the Department of Electromagnetic Field, FEE CTU in Prague, is in agreement.

In Prague, 25.05.2017

Contents

List of Used Abbreviations and Symbols	3
List of Figures	6
List of Tables.....	8
Introduction	9
1. FMCW Radar Basic Principles	10
2. Radar Sensors Concept	12
3. Calibrator Design – Theoretical Part.....	15
3.1. Calibrator concepts	15
3.2. Variations of the target RCS and the range to target.....	17
3.3. Influence of step phase change	20
4. Calibrator Design – Practical Realization	23
4.1. RF parts overview and description	23
4.2. PCB layout design	26
4.3. Components soldering, connectors mounting and shielded box placing 32	
4.4. Microcontroller choice and application software developing	34
5. Measurement and Experimental Results.....	36
5.1. S-parameters measurement.....	36
5.2. Microcontroller signal measurements	39
5.3. Signal spectrum measurement	40

5.4. Calibrator testing	42
Conclusions	49
References	50
Appendix A. Application Software Flowcharts.....	52
A.1. Main application flowchart	52
A.2. “User button pressed” interrupt flowchart	53
A.3. “TIM1 overflow” interrupt flowchart	54
Appendix B. Application Source Code Listing.....	55
B.1. Main program – <i>main.c</i>	55
B.2. Interrupt routine – <i>stm8l15x_it.c</i>	57

List of Used Abbreviations and Symbols

2D-FFT	Two Dimensional Fast Fourier Transform
AD	Active Defense
ADC	Analog-to-Digital Converter
GCPW	Grounded Coplanar Waveguide
CW	Continuous Wave
DC	Direct Current
FFT	Fast Fourier Transform
FM	Frequency Modulation
FMCW	Frequency Modulated Continuous Wave
FMICW	Frequency Modulated Interrupted Continuous Wave
HP	High-Pass
IC	Integrated Circuit
IF	Intermediate Frequency
IL	Insertion Loss
LFA	Low-Frequency Amplifier
LNA	Low-Noise Amplifier
LO	Local Oscillator
LP	Low-Pass
LSB	Least Significant Bit
MCD	Multi-Channel Decorrelator
MMIC	Monolithic Microwave Integrated Circuit
MOD	Modulator
PA	Power Amplifier
PCB	Printed Circuit Board

QFN	Quad-Flat No-leads
RCS	Radar Cross Section
RF	Radio Frequency
RL	Return Loss
RMS	Root Mean Square
Rx	Receiver
Tx	Transmitter
VCC	Power Supply Voltage
VNA	Vector Network Analyzer
c	the light velocity
Δt	phase shifter LSB switching time
f_0	central frequency of the radiated signal
f_D	the Doppler frequency shift
f_{IF}	IF frequency after mixer
$G_{c Rx}$	receiving antenna gain of the calibrator
$G_{c Tx}$	transmitting antenna gain of the calibrator
G_{Rx}	receiving antenna gain of the radar
G_{Tx}	transmitting antenna gain of the radar
$\varphi_{bb}(t)$	phase of filtered baseband signal of the CW radar in Rx chain
L_c	total loss of the calibrator
λ	wavelength of the transmitted signal
P_{rad}	power radiated from the CW radar
P_{rec}	power received from the target
R_c	range to the calibrator
R_t	the range to target

$s_{\text{bb}}(t)$	filtered baseband signal of the CW radar in Rx chain
σ_t	RCS of the target
τ	two-way propagation delay
v_r	the target radial velocity

List of Figures

Fig. 1. The frequency difference between the transmitted chirp (solid line) and the target echo (dashed line) and resulting IF frequency after the mixer.	11
Fig. 2. Block diagram of analog CW Doppler radar.....	12
Fig. 3. Block diagram of digitally-modulated CW Doppler radar.....	13
Fig. 4. Block diagram of the calibrator based on analog phase shifter [4].	16
Fig. 5. Block diagram of the designed calibrator.	16
Fig. 6. Target and the calibrator are located at the different ranges from radar.	18
Fig. 7. Illustration of step phase changes vs ideal case.....	20
Fig. 8. Spectrum of the simulating signals for a) $f_D = 2$ kHz; b) $f_D = 10$ kHz.	21
Fig. 9. The Qorvo TGP2109-SM phase shifter: a) functional block diagram; b) part top view.....	24
Fig. 10. The Macom MAAD-011021 attenuator functional schematic.....	25
Fig. 11. MAX850/MAX851/MAX852 adjustable configuration.	26
Fig. 12. Electrical schematics: a) attenuator; b) phase shifter.....	27
Fig. 13. Attenuator PCB layout: a) top layer view; b) bottom layer view.....	28
Fig. 14. Phase shifter PCB layout: a) top layer view; b) bottom layer view... ..	29
Fig. 15. Top layer of used GCPW with tapering shape.	30
Fig. 16. Simulated S-parameters of designed GCPW.....	31
Fig. 17. D-sub connector pin numbering.	32
Fig. 18. Phase shifter: a) top view; b) bottom view.....	33
Fig. 19. Attenuator: a) top view; b) bottom view.	33
Fig. 20. STM8L-Discovery board.....	34
Fig. 21. S-parameters measurement setup.	36
Fig. 22. Measured S-parameters of the phase shifter.....	37

Figure 23. Measured S-parameters of the attenuator.....	37
Fig. 24. Insertion loss for each significant bit.....	38
Fig. 25. Oscilloscope screenshots for: a) mode #1; b) mode #2; c) mode #3; d) mode #4.....	39
Fig. 26. Oscilloscope screenshots for: a) mode #5; b) mode #6.....	40
Fig. 27. Spectrum at: a) phase shifter input; b) phase shifter output.....	41
Fig. 28. Calibrator testing setup.	42
Fig. 29. Time domain waveform and corresponding FFT spectrum for simulating target with 25 m/s radial velocity.....	43
Fig. 30. Time domain waveform and corresponding FFT spectrum for simulating target with 50 m/s radial velocity.....	44
Fig. 31. Time domain waveform and corresponding FFT spectrum for simulating target with 75 m/s radial velocity.....	45
Fig. 32. Time domain waveform and corresponding FFT spectrum for simulating target with 110 m/s radial velocity.....	46

List of Tables

Table 1. Required attenuation	19
Table 2. MMIC Digital Phase-Shifters	23
Table 3. MMIC Digital Attenuators.....	23
Table 4. D-sub pins and PCB pads correspondence	32
Table 5. Program modes and its parameters.	35
Table 6. Error of pseudo-Doppler frequency.	47

Introduction

FM radars represent one of the oldest and simplest – yet at the same time one of the most versatile types of radar. The use of frequency modulation to obtain range information in radar is almost as old as radar itself, dating back to 1924 when Appleton and Barnett used the technique for ionospheric sounding. The principles are very simple, yet FM radar have some interesting and elegant properties that make them very well suited to a number of specialist applications [1].

Nowadays, FMCW (frequency modulated continuous wave) and FMICW (frequency modulated interrupted wave) radars have received a great deal of popularity by the military and automotive industries by virtue of their simplicity, high reliability and low cost. The continuous wave, which is well matched to simple solid-state transmitter, employs low continuous power compared to the high peak power of pulsed radar for the same detection performance. The dechirp-on-receive operation greatly reduces the ADC sampling rate, the ADC realization is simplified as a result.

Apart from design such types of radar there is necessary in development of a radar target simulator for their calibration, testing and characterization. The presented paper describes concept and design of such digital-controlled MMIC based devices, simulating moving targets with a well-defined radial velocity up to 75 m/s within the 8-12 GHz frequency band for active defense (AD) system.

1. FMCW Radar Basic Principles

Consider, in its simplest form, the FMCW radar. The transmitted waveform of this radar has a constant amplitude, but a linear sawtooth variation of frequency with time. The linear variation of frequency with time is often referred to as *chirp*. A moving target echo (see Fig. 1) will consist of a replica of this transmitted waveform, delayed by the two-way propagation delay:

$$\tau = 2R_t/c, \quad (1)$$

where R_t – the target range and c is the light velocity and shifted in frequency by the Doppler frequency shift:

$$f_D = -2v_r f_0/c, \quad (2)$$

where v_r – the target radial velocity and f_0 is central frequency of the transmitted signal. After a direct downconversion by the mixer to the baseband at 0 Hz the resulting IF frequency (or beat frequency) can be obtained from:

$$f_{IF} = 2mR_t/c + 2v_r f_0/c, \quad (3)$$

where m – the slope of the frequency ramp.

From this relation it is quite obvious that a separation of distance and velocity is not possible from a single ramp. Thus, multiple ramps with different slopes have to be used followed by a matching of detected objects. However, depending on the situation and modulation scheme this can lead to ambiguities in combination with a significant computational effort for object matching. An alternative modulation scheme which avoids these ambiguities is the chirp sequence modulation.

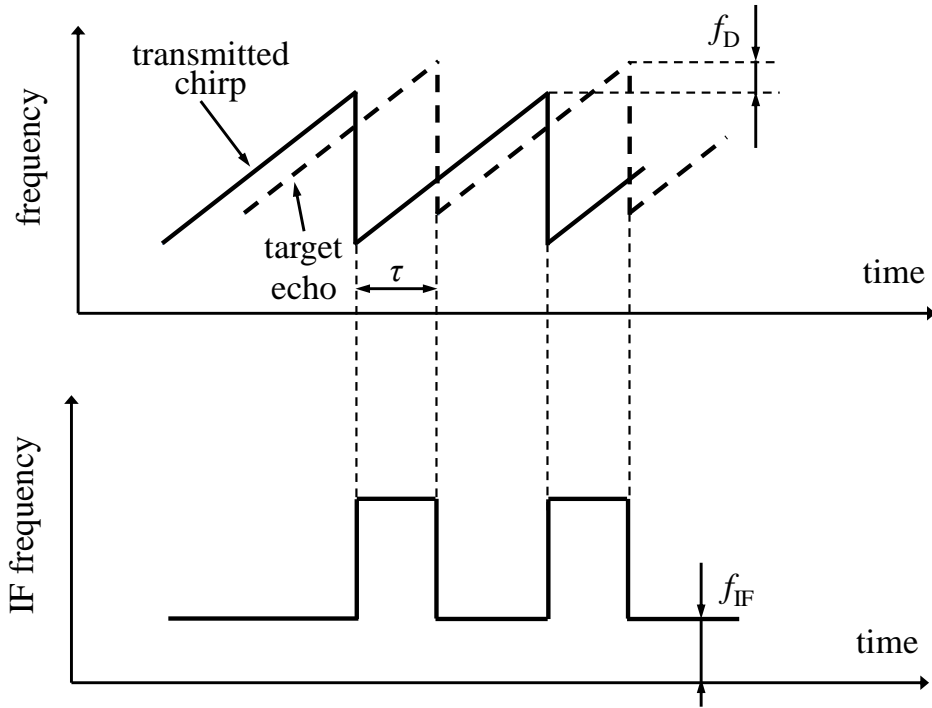


Fig. 1. The frequency difference between the transmitted chirp (solid line) and the target echo (dashed line) and resulting IF frequency after the mixer.

A chirp sequence consists of a large number of fast frequency ramps with the chirp duration T_{chirp} and denoting N as the number of chirps. The signal processing of such a chirp sequence is accomplished in the following way: First a FFT is performed for each single chirp yielding the distance range of a detected object. Due to the high slope of the frequency ramp the frequency shift term due to the Doppler effect is by far smaller than the range shift within one chirp. However, from chirp to chirp the phase changes due to the Doppler effect. Therefore, in the following step a second FFT is performed for each distance range across the single chirps [3]. Thus, the 2D-FFT shows the distance range on one coordinate and the velocity of the object on the other one.

2. Radar Sensors Concept

As we said, the designed calibrator serves for radar sensors for AD system [2]. In general, the AD systems are based on detection of approaching threat missiles and activation of suitable counter-missiles able to destroy, deflect or de-activate the former one. For these purposes, it is beneficial to employ the CW radars. The main advantage radars of this type is their ability to detect fast flying targets and easily suppress stationary or slow moving ones. The HW elimination of stationary and low-frequency signal leads to substantial improvement in the radar dynamic range. But as a result, the corresponding CW radars can be tested and measured only by utilizing moving targets. This can be expensive and time-consuming, especially in case of testing AD systems by means of real military missiles.

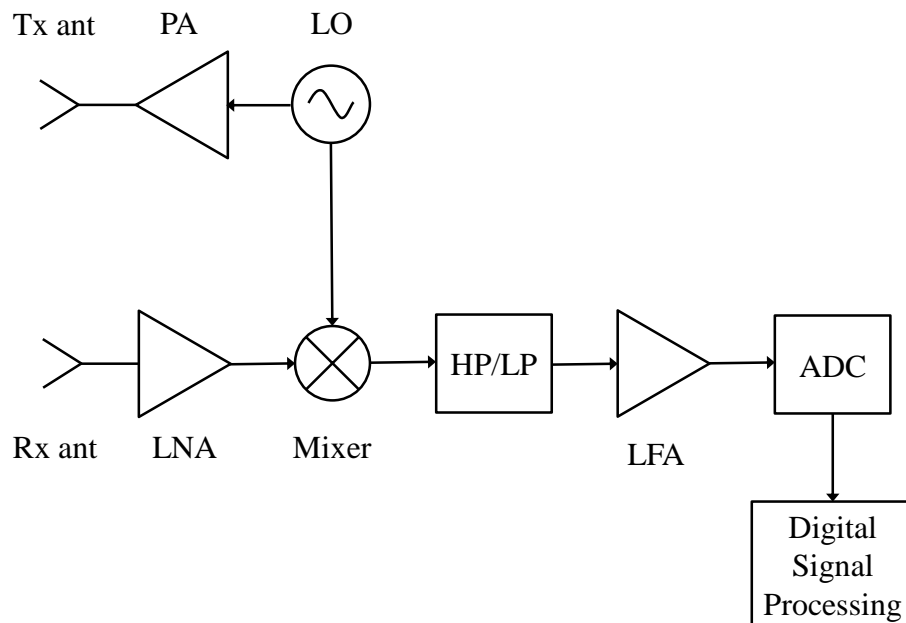


Fig. 2. Block diagram of analog CW Doppler radar.

The block diagram of basic analog CW radar is shown in Fig. 2. The target is illuminated by a CW produced by local oscillator (LO), amplified by power amplifier (PA) and radiated through transmitting antenna. The receiver is based on a coherent mixing of the received and amplified signal downconverted in the mixer to the baseband. After removing the DC component by means of high-pass filter signal is amplified again by low-frequency amplifier (LFA) with high gain. It allows us to detect the moving targets with a very high sensitivity.

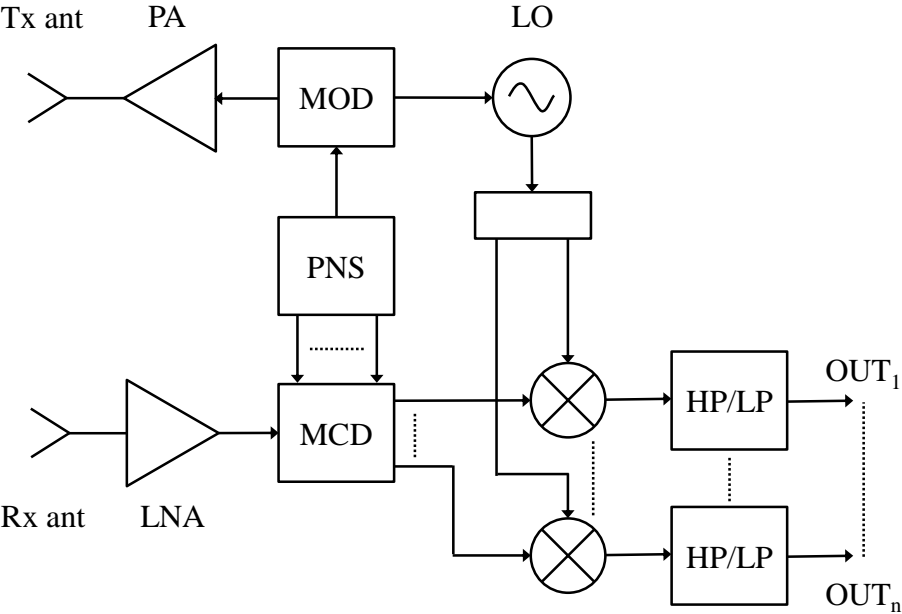


Fig. 3. Block diagram of digitally-modulated CW Doppler radar.

Fig. 3 show us the block diagram of more complex digitally modulated CW radar. The transmitted wave has frequency modulation performed in the modulator (MOD) driven by pseudo-noise sequence (PNS) generator. The receiver performs the correlation of the received signal with several time-shifted PN sequences in the multi-channel decorrelator (MCD). Then the decorrelated signals are downconverted into baseband and subsequently filtered and amplified in the same way as in case of the analog structure. The additional

modulation and correlation processes contribute to a substantial rise in immunity of the radar against interfering signals and allow us to perform the range measurements. Although the removal of all static reflections and cross-talks results in a considerable increase of the radar dynamic range, it also makes the system measurements and testing procedure more difficult to implement.

3. Calibrator Design – Theoretical Part

3.1. Calibrator concepts

Possible calibrator concept can be derived from principles of the basic CW radar shown in Fig. 2. The main idea behind that is to simulate baseband signal $s_{bb}(t)$ of the CW radar at the HP/LP filter output which can be described as follows:

$$s_{bb}(t) = A_{bb} \cos[\varphi_{bb}(t)] = A_{bb} \cos[2\pi f_D t + \varphi_0] \quad (4)$$

where A_{bb} – amplitude of the baseband signal which depends on the amplitude of the transmitted signal, RCS of the target, propagation losses and conversion gain of the CW radar receiver; φ_0 – phase shift due to the range to target.

In order to obtain the output signal of the calibrator simulating constant target radial velocity, baseband signal phase $\varphi_{bb}(t)$ must changes linear with time (for simplicity let's assume that the range to target is 0 m):

$$\varphi_{bb}(t) = 2\pi f_D t. \quad (5)$$

Such a linear phase change can be realized in various ways. One of these simple methods is shown in Fig. 4. Either short- or open-ended from one side an analog phase shifter is connected to the antenna input. The analog phase shifter is controlled by the microcontroller DAC signal. The signal received by the antenna (best to use an aperture antenna) will be reflected with a phase shift $2\varphi_{bb}$, where this phase shift is time-changing and set from 0 to 180. Realization and experimental testing of such calibrator type is described in [4].

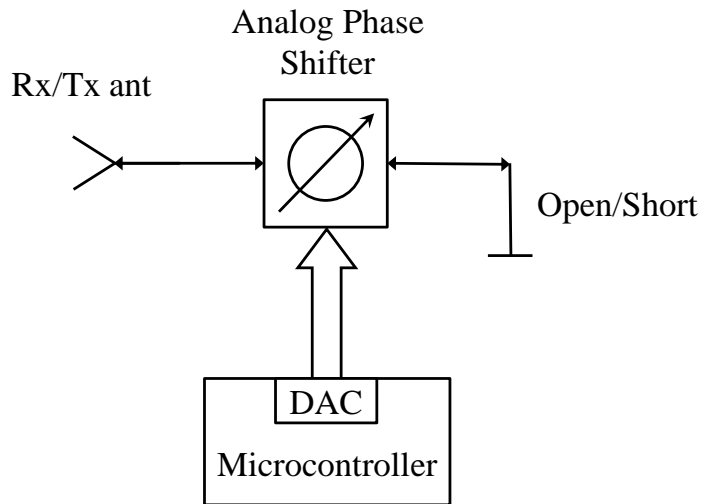


Fig. 4. Block diagram of the calibrator based on analog phase shifter [4].

This work is dedicated to realization of another calibrator type which structure is illustrated on Fig. 5.

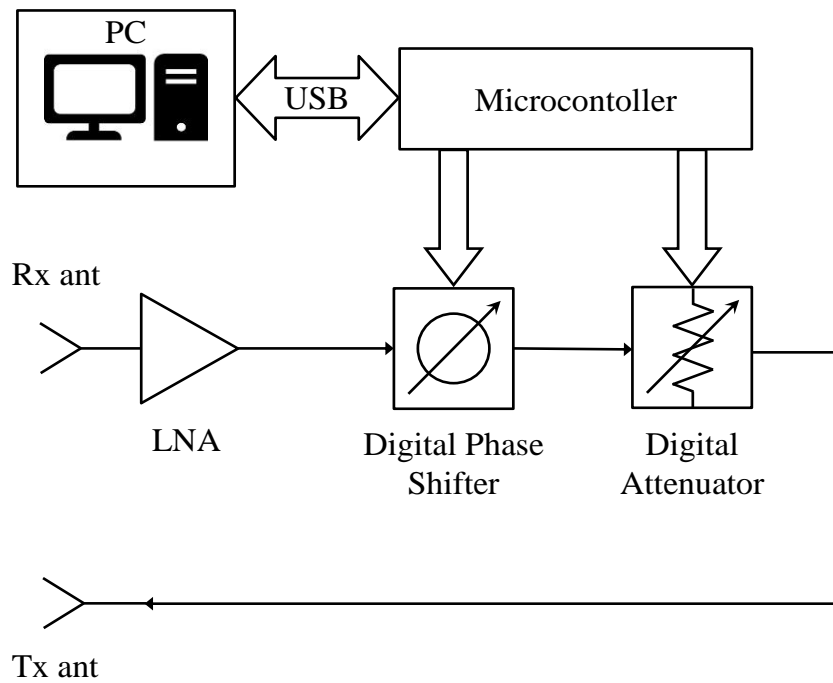


Fig. 5. Block diagram of the designed calibrator.

The structure is based on the digital MMIC step phase-shifter and digital MMIC step attenuator controlled by the microcontroller. The incident wave from the radar is received by the Rx antenna, passes through the calibrator, radiated in the direction to the radar by the Tx antenna and goes the same way back. Low noise amplifier, as we will see in the following subsection, may be required for simulating target with high RCS and located at close distances.

Because this structure is using step phase-shifter as a core component it's necessary to know required time Δt , during that time the digital step phase-shifter should switch its phase by $\Delta\varphi_{bb}$. Using formulas (5) and (2) and taking into account that Doppler frequency shift occurs twice at radar we obtain:

$$\Delta t = \frac{\Delta\varphi_{bb}}{\pi f_D} = \frac{\Delta\varphi_{bb} c}{2\pi v_r f_0} \quad (6)$$

For example, for the 11 GHz radar, the calibrator based on the 6-bit phase-shifter with resolution 5.625° and assuming that simulation target should have radial velocity 100 m/s it gives us required 4.26 μ s between phase switches.

3.2. Variations of the target RCS and the range to target

Now let us look what gain (or loss) the calibrator must add to received signal from the radar to simulate the target RCS and the range to the target. For this purpose, consider case of presence real target and case of a calibrator (Fig. 6).

Writing radar equation for case of the target we obtain:

$$P_{\text{rec}} = \frac{P_{\text{rad}} G_{\text{Tx}} G_{\text{Rx}} \sigma_t \lambda^2}{(4\pi)^3 R_t^4}, \quad (7)$$

where P_{rec} – received power from the target, P_{rad} – radiated power of the radar, G_{Tx} – transmitting antenna gain of the radar, G_{Rx} –receiving antenna gain of the radar, σ_t – RCS of the target, R_t – the target range and λ – wavelength of the transmitted signal.

In a case of calibrator instead of the target radar equation looks as:

$$P_{\text{rec}} = \frac{P_{\text{rad}} G_{\text{Tx}} G_{\text{Rx}} G_{\text{c Tx}} G_{\text{c Rx}} \lambda^4}{(4\pi R_c)^4 L_c}, \quad (8)$$

where $G_{\text{c Rx}}$ – receiving antenna gain of the calibrator, $G_{\text{c Tx}}$ – transmitting antenna gain of the calibrator, R_c – range to the calibrator and L_c – total loss of the calibrator.

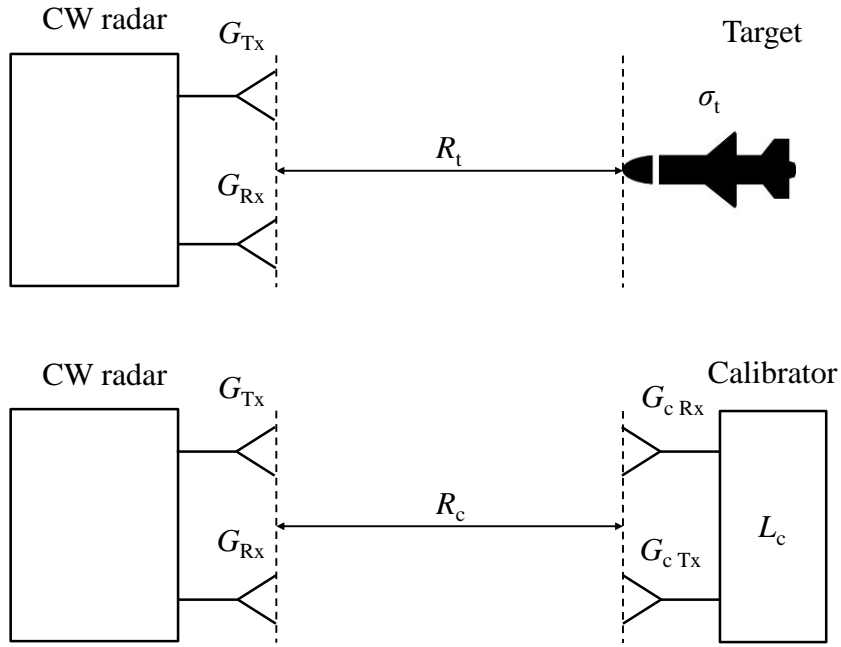


Fig. 6. Target and the calibrator are located at the different ranges from radar.

Now, taking into account that these received powers in both cases must be equal, we can obtain required total loss of the calibrator L_c for given target RCS σ_t and range to the target R_t :

$$L_c = \frac{G_{c \text{ Rx}} G_{c \text{ Tx}} \lambda^2}{2\pi\sigma_t} \cdot \left(\frac{R_t}{R_c}\right)^4. \quad (9)$$

As we seen before calibrator consists from phase-shifter and attenuator, so we can roughly express $L_c = L_{\text{ph.shifter}} + L_{\text{att}}$, where $L_{\text{ph.shifter}}$ – loss of the phase-shifter and L_{att} – loss of the attenuator.

Table 1. Required attenuation

R_t [m]	σ_t [m ²]	L_c [dB]	L_{att} [dB]
1	10^{-4}	12.7	5.7
	10^{-3}	2.7	-4.27
	10^{-2}	-7.27	-14.7
10	10^{-4}	52.7	45.7
	10^{-3}	42.7	35.7
	10^{-2}	32.7	25.7

Required L_c and L_{att} are shown in the Table 1 for simulating targets at the distances 1 m and 10 m with RCS fluctuating from 10^{-4} to 10^{-2} m² for 11 GHz radar and assuming that the calibrator are located $R_c = 1$ m from the radar, $L_{\text{ph.shifter}} = 7$ dB and $G_{c \text{ Rx}} = G_{c \text{ Tx}} = 6$ dBi.

3.3. Influence of step phase change

Since we use digital phase shifter with step changes of phase it results in parasitic phase modulation which the calibrator adds to the received signal from the radar apart from frequency Doppler shift (Fig. 7).

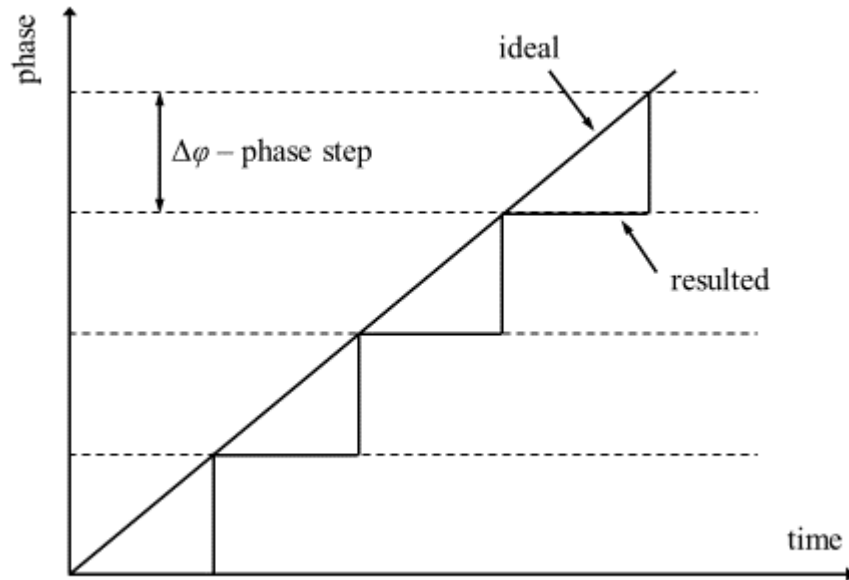
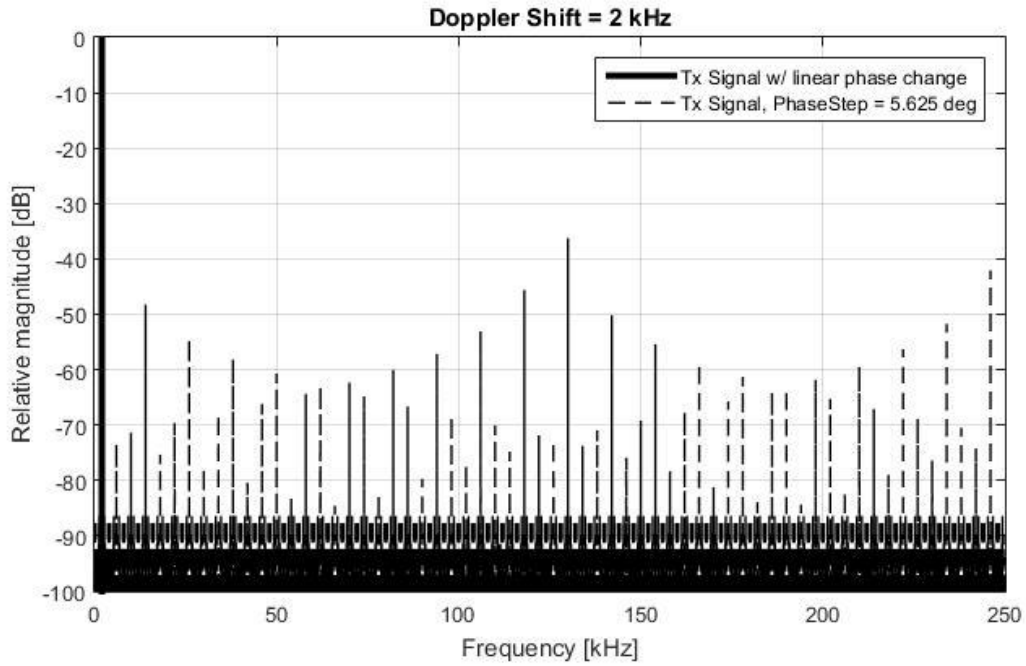


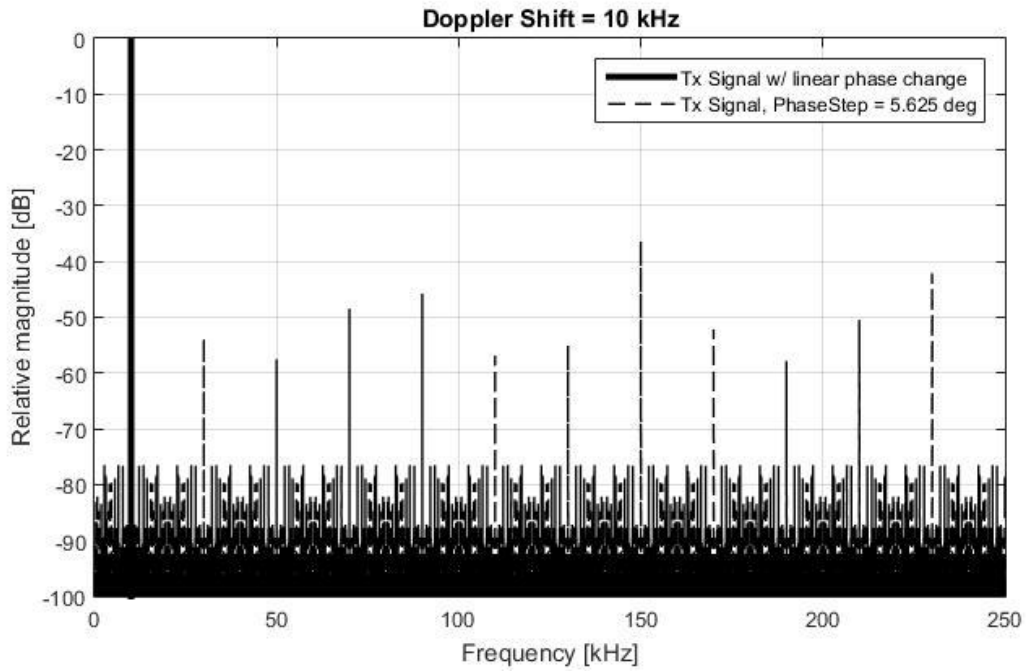
Fig. 7. Illustration of step phase changes vs ideal case.

Therefore Fig. 8 shows the simulation results done in Matlab for phase step change at different Doppler frequencies shifts comparing with the required ideal linear phase ramp.

Analyzing resulting spectrum of the baseband signal with step phase changes we can conclude that this parasitic phase modulation adds many side harmonics which are located at the frequencies $f_D (2n + 1)$, $n = 1, 2, 3, \dots$, and minimum difference in levels between harmonics is 36 dB.



a)



b)

Fig. 8. Spectrum of the simulating signals for a) $f_D = 2$ kHz; b) $f_D = 10$ kHz.

It means that in case of simulating targets with low velocities (Doppler frequency shift values result in several kHz) these harmonic can pass through

HP/LP filter of the radar and cause unwanted distortion of baseband signal.
However, real-world measurements are required.

4. Calibrator Design – Practical Realization

4.1. RF parts overview and description

The next step after defining concept of the radar calibrator is searching for suitable components of the future devices. Main characteristics of the possible digitally controlled MMICs which fit to 11 GHz band are illustrated in Table 2 and Table 3 [5-10].

Table 2. MMIC Digital Phase-Shifters

Name	Manufacturer	Resolution	Price, \$
HMC642A	Analog Devices	6 bits/5.6 °	102.69
MAPS-010166	MACOM	6 bits/5.6 °	89.95
TGP2109-SM	QORVO	6 bits/5.6 °	84

Table 3. MMIC Digital Attenuators

Name	Manufacturer	Step/Range, dB	Price, \$
HMC1018A	Analog Devices	1/31	89.64
MAAD-011021	MACOM	0.5/31.5	68
TGP2226-SM	QORVO	0.5/31.5	50

For reasons of price and practical realization, TGP2109-SM from Qorvo for phase-shifter realization and MAAD-011021 from Macom for attenuator realization were chosen.

The Qorvo TGP2109-SM is a packaged 6-bit bi-directional digital phase shifter fabricated on Qorvo's high performance 0.15 μ m GaAs pHEMT process [6]. It operates over 8 to 12 GHz and provides 360° of phase coverage with a LSB of 5.625°. It also achieves a low RMS phase error of 4° with 6 dB of insertion loss. Functional block diagram and part view in QFN package is shown on Fig. 9.

The Macom MAAD-011021 is a wide band 6-bit digital attenuator covering DC to 30 GHz [10]. The attenuation bit-values are 0.5 dB LSB, 1, 2, 4, 8, and 16 dB for a total attenuation of 31.5 dB. Attenuation error is typically less than +/- 0.5 dB, RMS phase error is less than 5 degrees at 20 GHz, and typical insertion loss is 7.2 dB at 15 GHz. Return loss is typically 12 dB across all frequencies and attenuation states. Functional schematic is illustrated on Fig. 10.

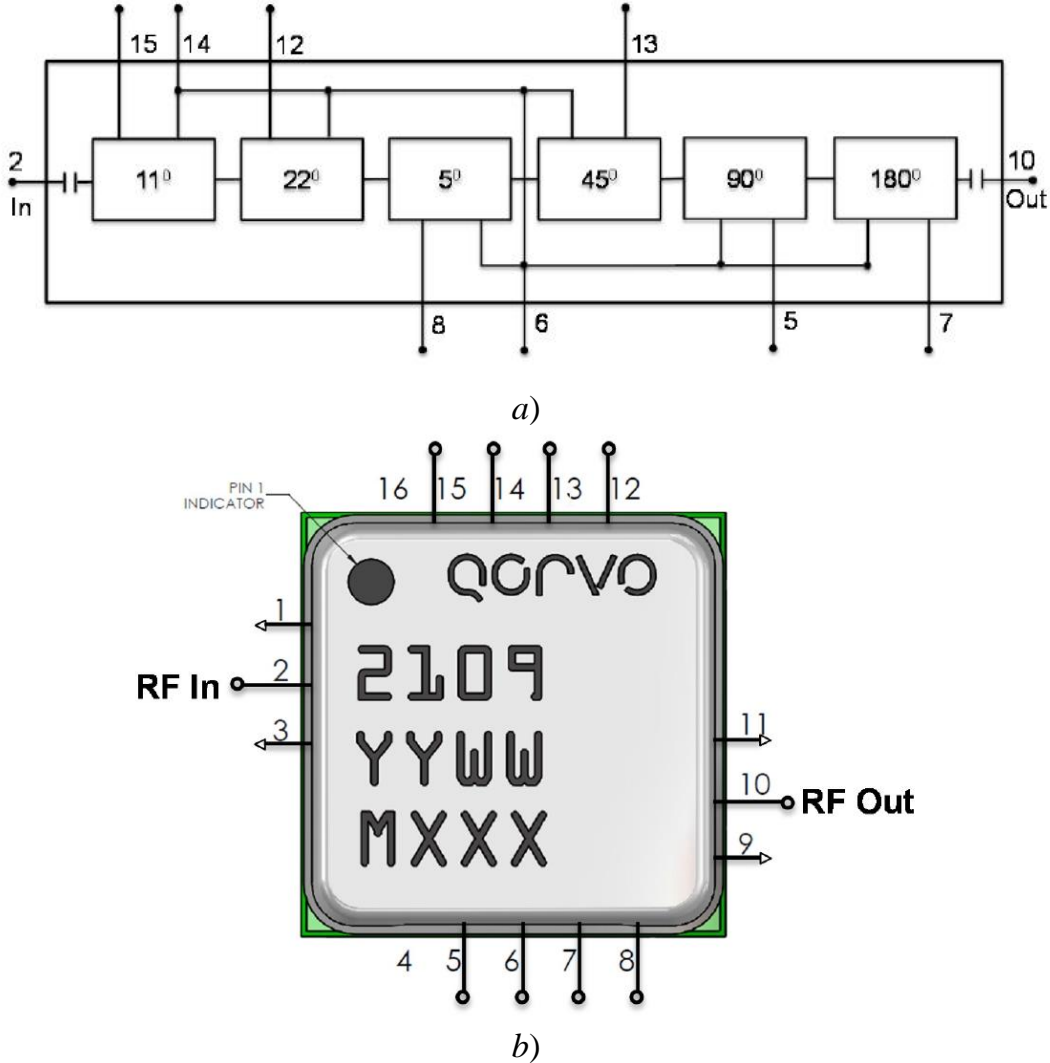


Fig. 9. The Qorvo TGP2109-SM phase shifter: a) functional block diagram; b) part top view.

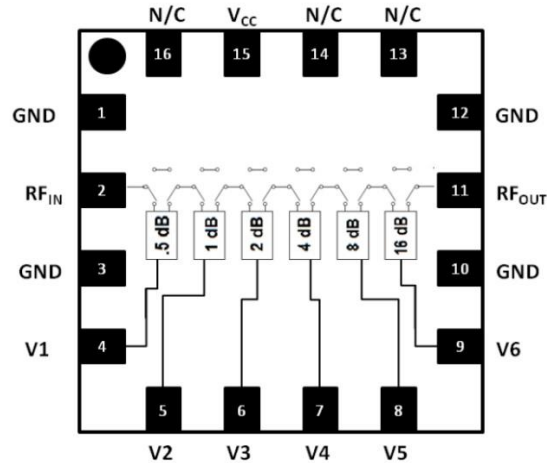


Fig. 10. The Macom MAAD-011021 attenuator functional schematic.

The attenuator integrates an inverter to allow a single control for series/shunt attenuation. This inverter requires a -5 V supply (VCC) and 17 mA typical, logic is 0 V / +5 V.

For this -5 V VCC realization circuit based on MAX851 IC was implemented (Fig.11). The Maxim MAX851 is low-noise inverting charge-pump power supply which offers adjustable (-0.5 V to -9 V) output voltages [11]. To provide required -5 V 1 % tolerant SMD resistors $R1 = 100 \text{ k}\Omega$ and $R2 = 290 \text{ k}\Omega$ from Yageo [12] for voltage divider were chosen according to datasheet recommendations. Tantalum Polymer SMD capacitors from Vishay [13] were used for C1, C2, C3 and C4 polar capacitors.

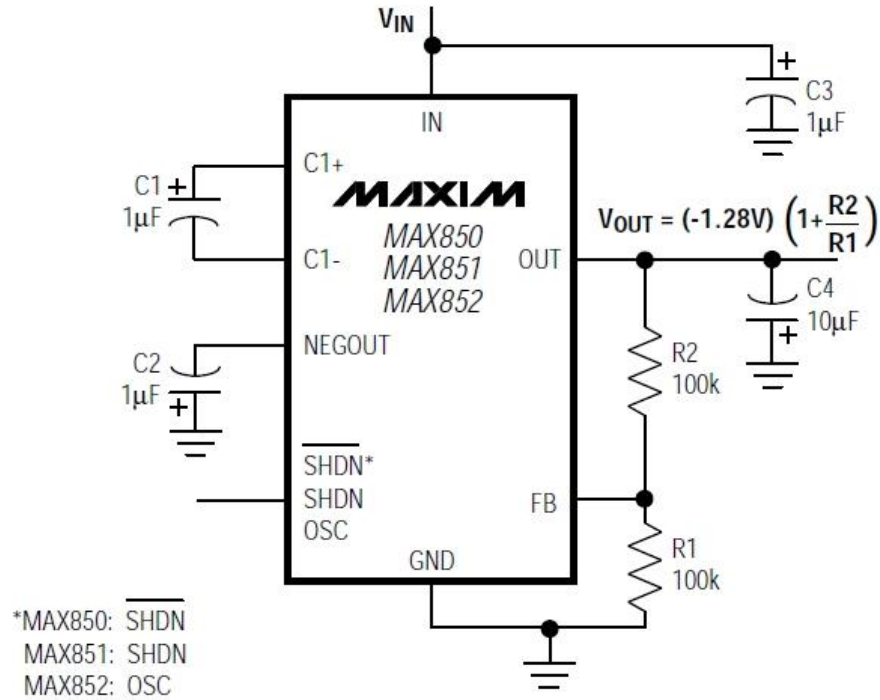
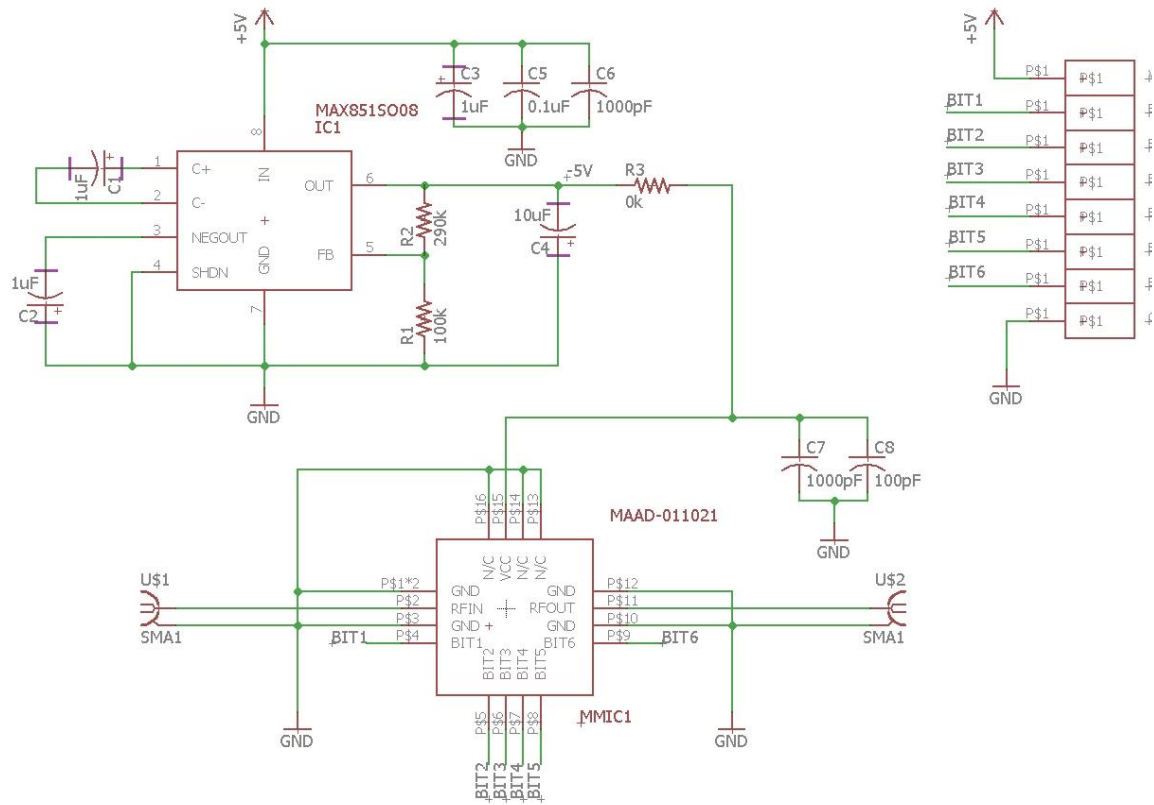


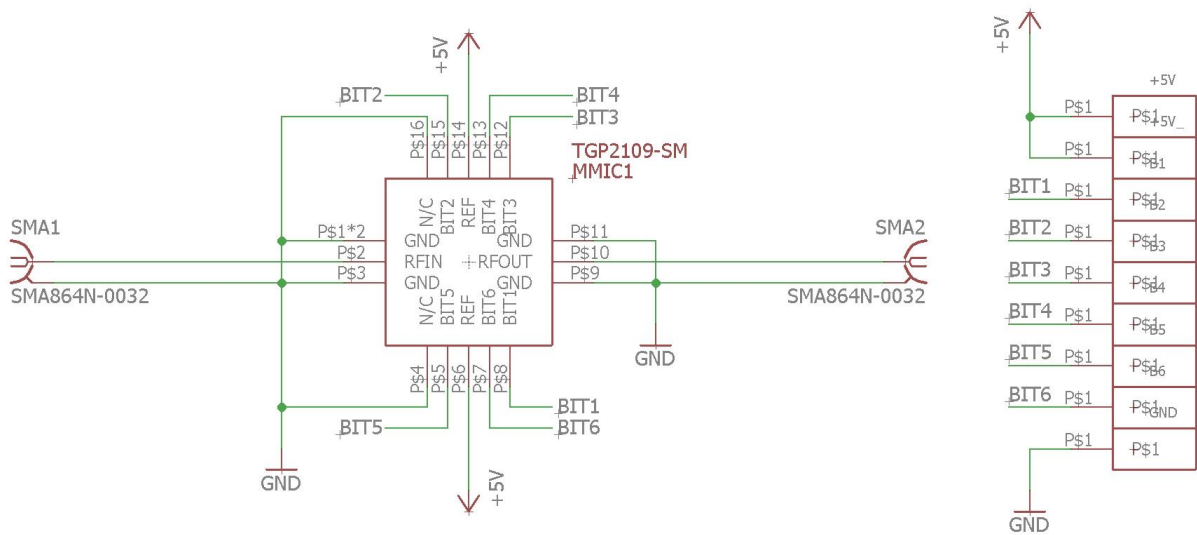
Fig. 11. MAX850/MAX851/MAX852 adjustable configuration.

4.2. PCB layout design

Electrical schematics (Fig. 12) and PCB layouts for both devices (Fig. 13 and Fig. 14) were drawn and designed in free version of Autodesk Eagle 7.7.0 software. This version is suitable for students and includes 2 schematic sheets, 2 signal layers, and 80 cm² board area. In addition, separate library with MMICs footprint for their proper soldering was created. For more details about schematics and layout view, please look into materials from CD (including Gerber files). All PCBs were manufactured by PragoBoard s.r.o. [14] in Prague.

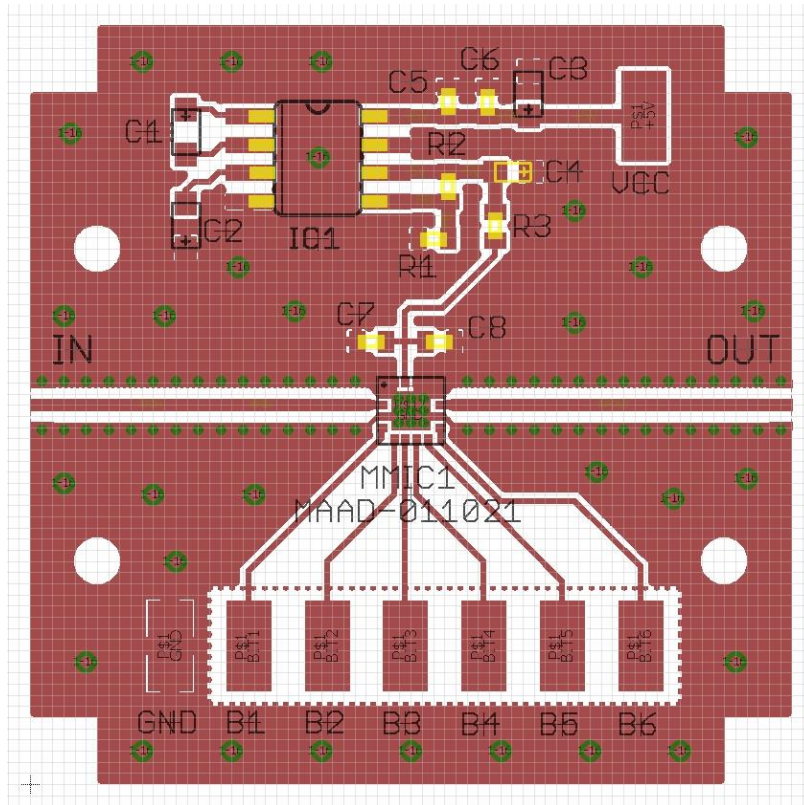


a)

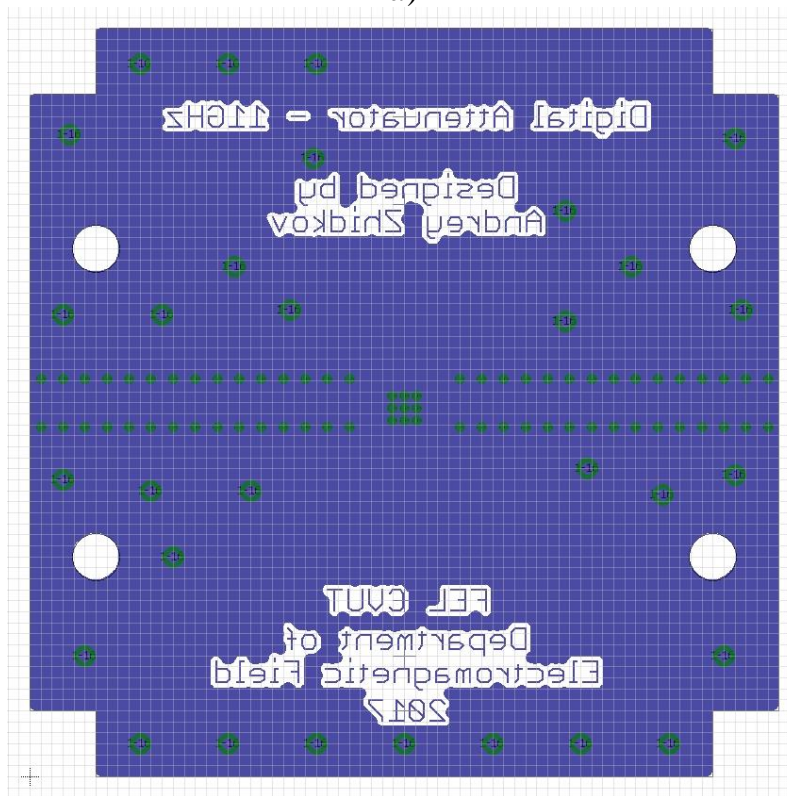


b)

Fig. 12. Electrical schematics: a) attenuator; b) phase shifter.

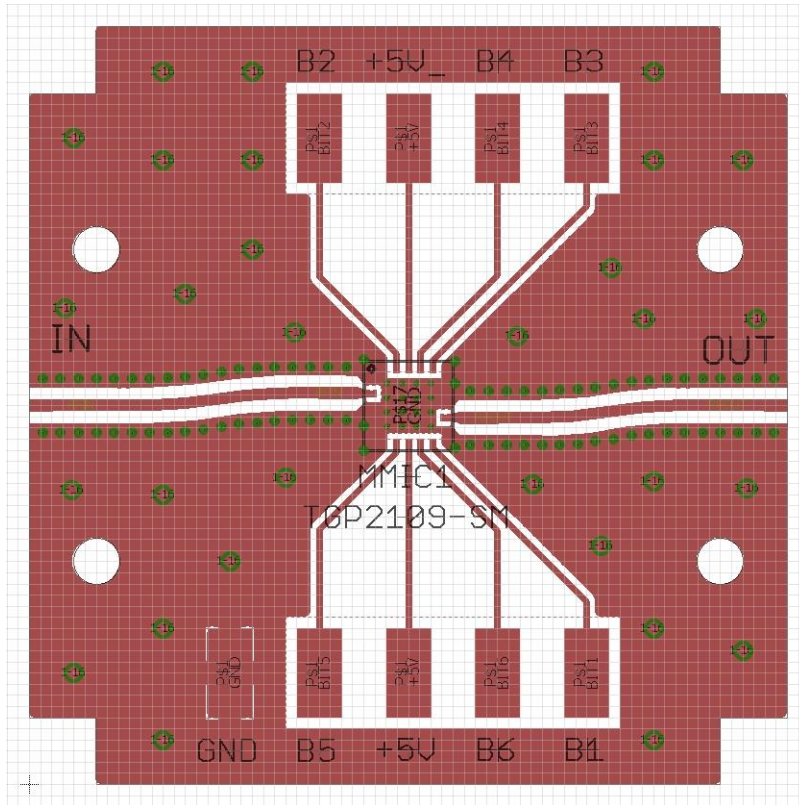


a)

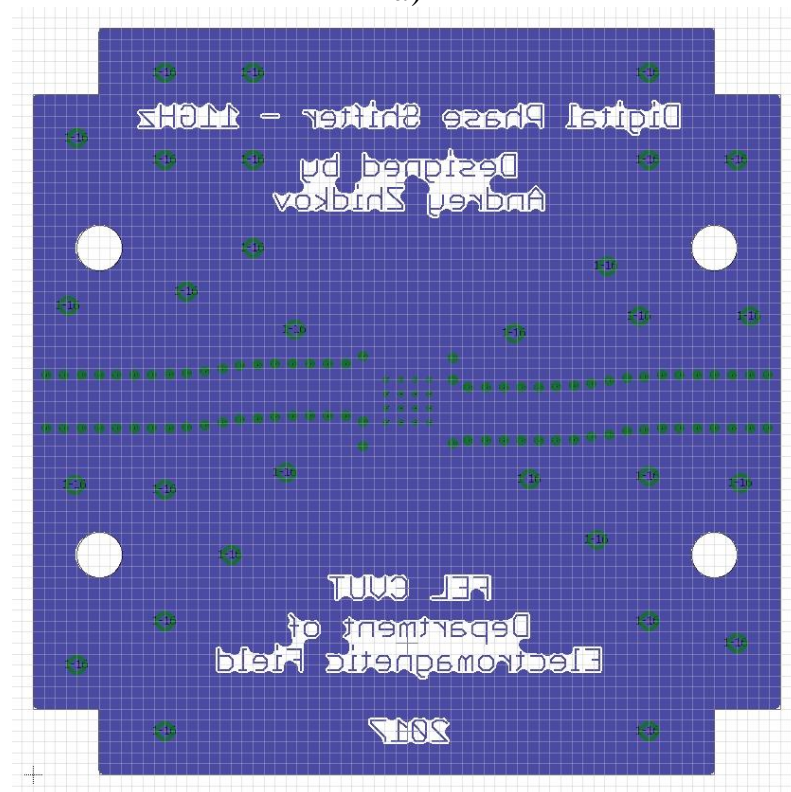


b)

Fig. 13. Attenuator PCB layout: a) top layer view; b) bottom layer view.



a)



b)

Fig. 14. Phase shifter PCB layout: a) top layer view; b) bottom layer view.

RF paths on both PCBs were realized in the form of GCPW having 50Ω characteristic impedance with 0.5 mm width and 0.55 mm gap and ending with 0.4 mm long tapering to connect 0.3 mm RFIN/RFOUT MMIC pads (Fig. 15). In order to ensure that such tapering does not affect the line impedance, a simulation in AWR Microwave Office was performed with results are shown in the Fig. 16.

All this GCPWs are assumed to be manufactured on Rogers 4350B substrate [15] with 0.508 mm thickness and $18 \mu\text{m}$ Cu metallization.

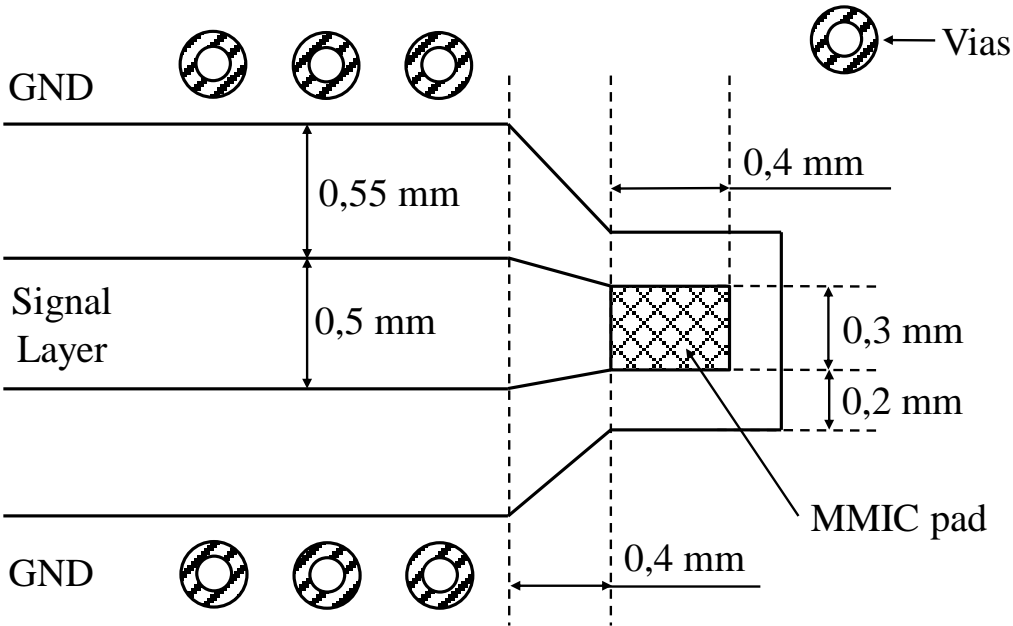


Fig. 15. Top layer of used GCPW with tapering shape.

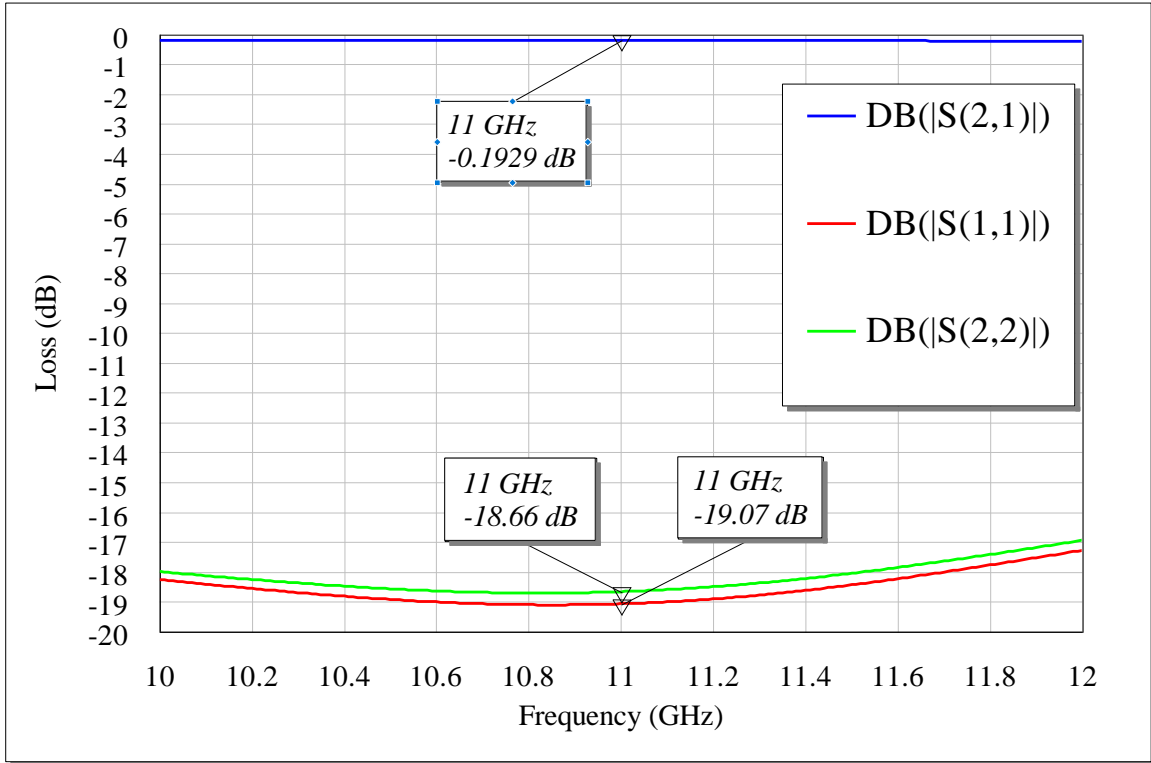


Fig. 16. Simulated S-parameters of designed GCPW.

4.3. Components soldering, connectors mounting and shielded box placing

MMIC components were soldered using hot air with PCB placed on a heated surface. Other components were soldered using common soldering station. After component soldering, PCBs, Jyebao SMA864N-0032 RF connectors [16] and usual D-sub 9 female connectors (Fig. 17) for power supply and controlling signals were mounting by screws on/into special aluminum boxes. Correspondence between D-sub 9 pins and PCB pads for both devices listed below in Table 4. Photos of the assembled devices without top and bottom metallic caps is shown on Fig. 14 and Fig. 15.

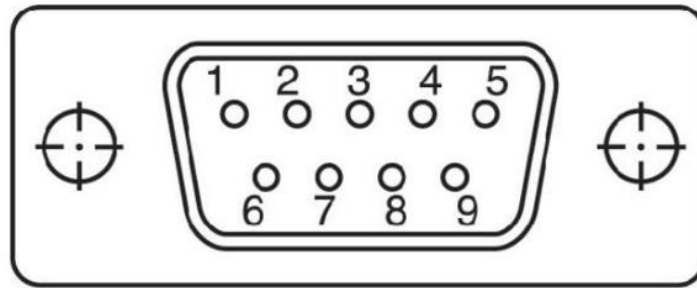
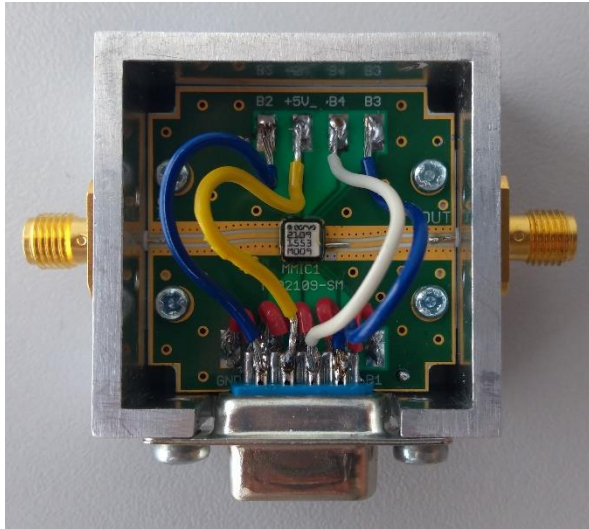


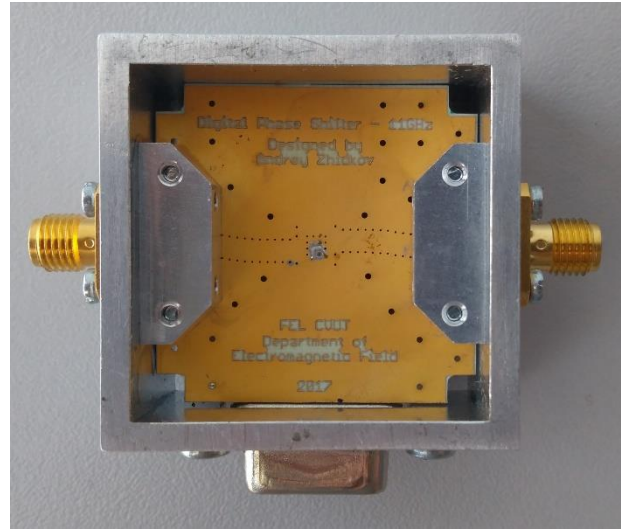
Fig. 17. D-sub connector pin numbering.

Table 4. D-sub pins and PCB pads correspondence

D-sub pin number	Phase shifter PCB pad name	Attenuator PCB pad name
1	GND	GND
2	B5	B1
3	+5V	B2
4	B6	B4
5	B1	B5
6	B2	VCC
7	+5V	B3
8	B4	B6
9	B3	N/C

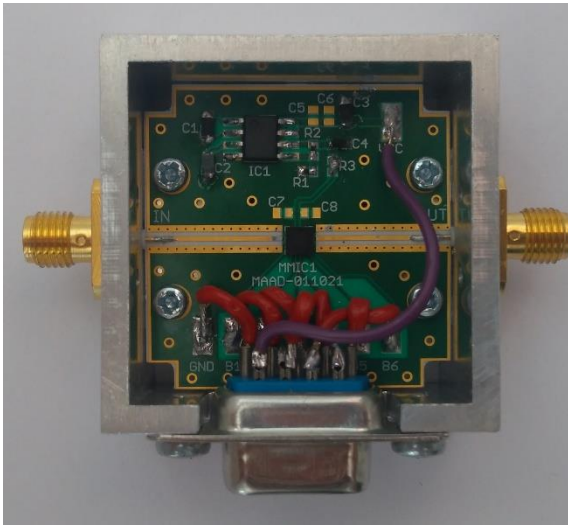


a)

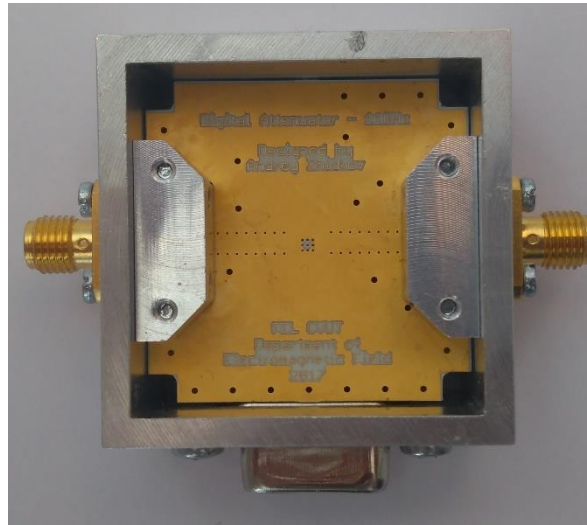


b)

Fig. 18. Phase shifter: a) top view; b) bottom view.



a)



b)

Fig. 19. Attenuator: a) top view; b) bottom view.

4.4. Microcontroller choice and application software developing

For application software developing, STM8L-Discovery board (Fig. 20) was provided by my supervisor. The board is based on STM8L152C6T6 microcontroller which is 8-bit ultra-low-power MCU, up to 64 KB Flash, with 2 KB data EEPROM, RTC, LCD, timers, USARTs, I2C, SPIs, ADC, DAC, comparators [17].



Fig. 20. STM8L-Discovery board.

The application program was written in C language using ST Visual Develop and Cosmic Compiler development tools. Due to the limited capabilities of STM8L-Discovery board, namely only one available user button (blue button on Fig. 16) program was written in the way that the interrupt from pushing the user button was used by microcontroller to change between simulating velocities.

After the microcontroller is switched on by connecting USB cable to the board or using some external power supply, the program is set to a mode #0 at which phase shifting MMIC is set to a constant phase shift of 0 degrees (this mode is

also used to measure S-parameters). After pressing the button again, the program switches to mode #1 and starts to simulate the target with radial velocity of 1 m/s. Further button pressing increases simulating speed and, once the maximum speed is reached, it switches back to mode #1. Corresponding simulated radial velocity, resulted Doppler frequency shift and LSB switching time for each mode are shown in Table 5.

Table 5. Program modes and its parameters.

Mode	Simulated v_r , m/s	Expected f_D , Hz	LSB switch time, μs
0	0	0	0
1	1	74	213
2	10	740	21.3
3	25	1850	8.5
4	50	3700	4.26
5	75	5550	2.84
6	110	8125	1.94

To increase MMIC phase by smallest phase step of 6.625, application uses microcontroller 16-bits timer TIM1 [18] and switching between phases happens at TIM1 overflow event. For more details about application flowchart structure and source code please refer to Appendix A and Appendix B respectively, or to materials on CD.

As already mentioned, the microcontroller has some limitations, so in the case of the attenuator it was decided to set the specified attenuation manually, applying control voltage to the corresponding pins.

5. Measurement and Experimental Results

5.1. S-parameters measurement

S-parameters of designed devices were measured by Agilent E8364A VNA calibrated from 10 GHz to 12 GHz (Fig. 21). Test conditions for phase shifter were 3 V supply voltage direct from microcontroller and MMIC phase set to 0° and 5 V supply voltage from power supply for attenuator at room temperature. Measurements results were processed and plotted in AWR Microwave Office software.

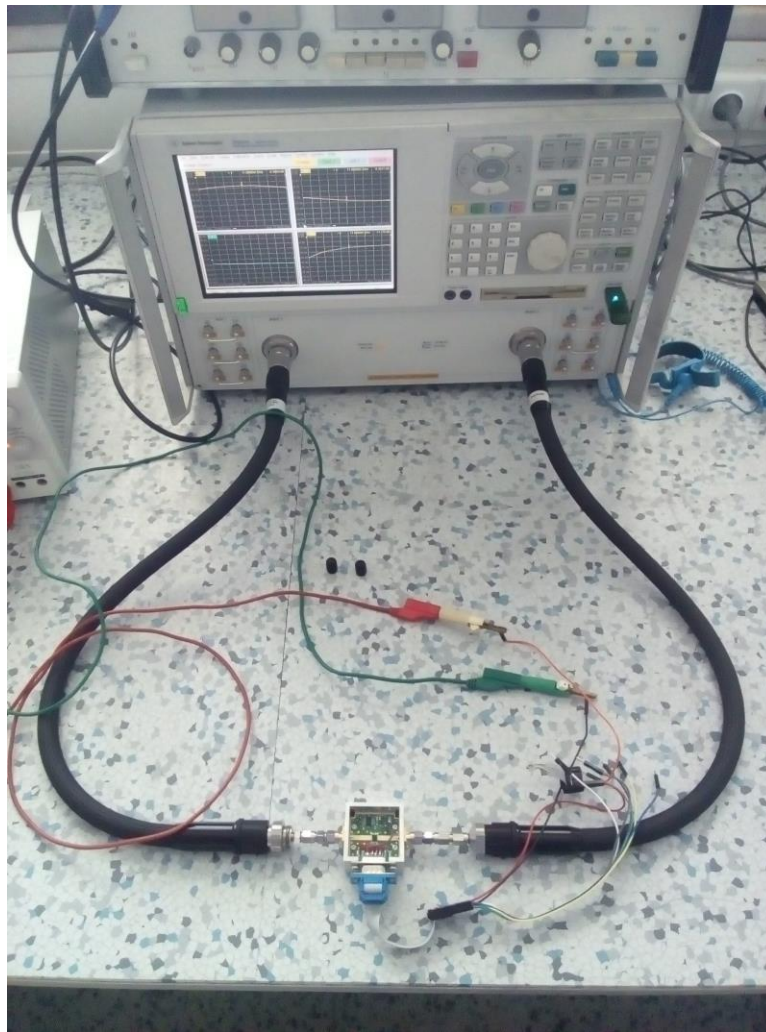


Fig. 21. S-parameters measurement setup.

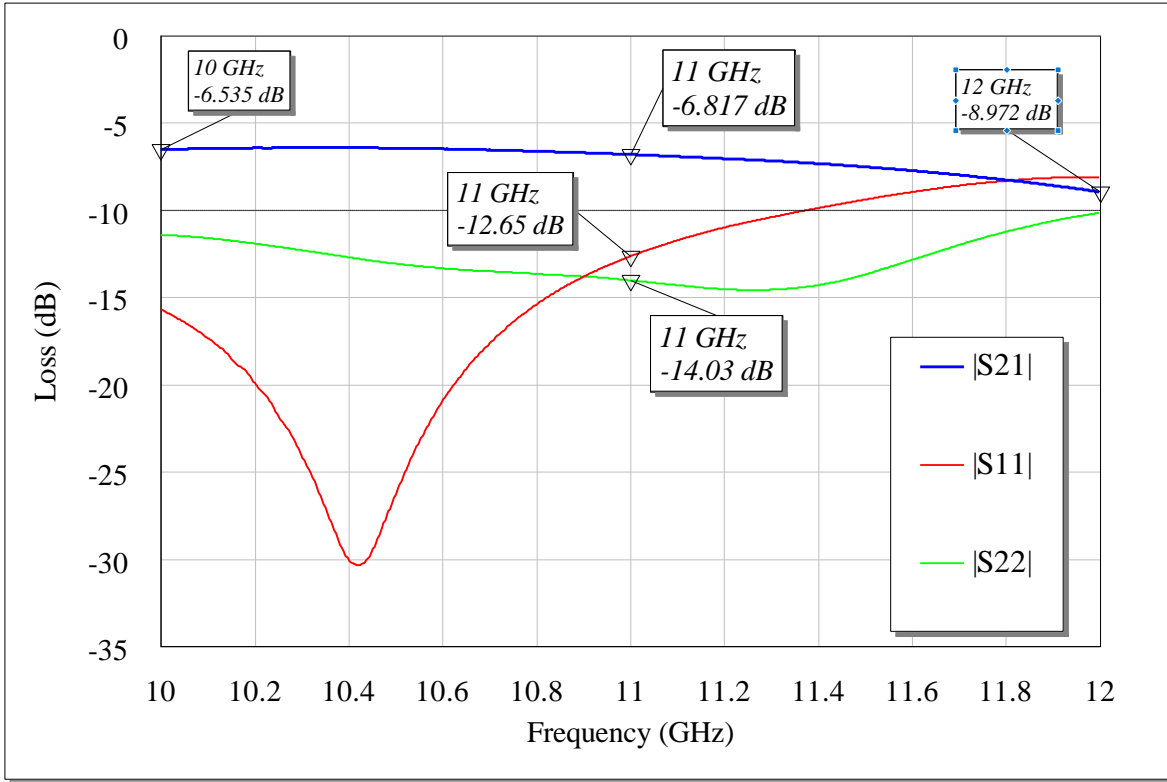


Fig. 22. Measured S-parameters of the phase shifter.

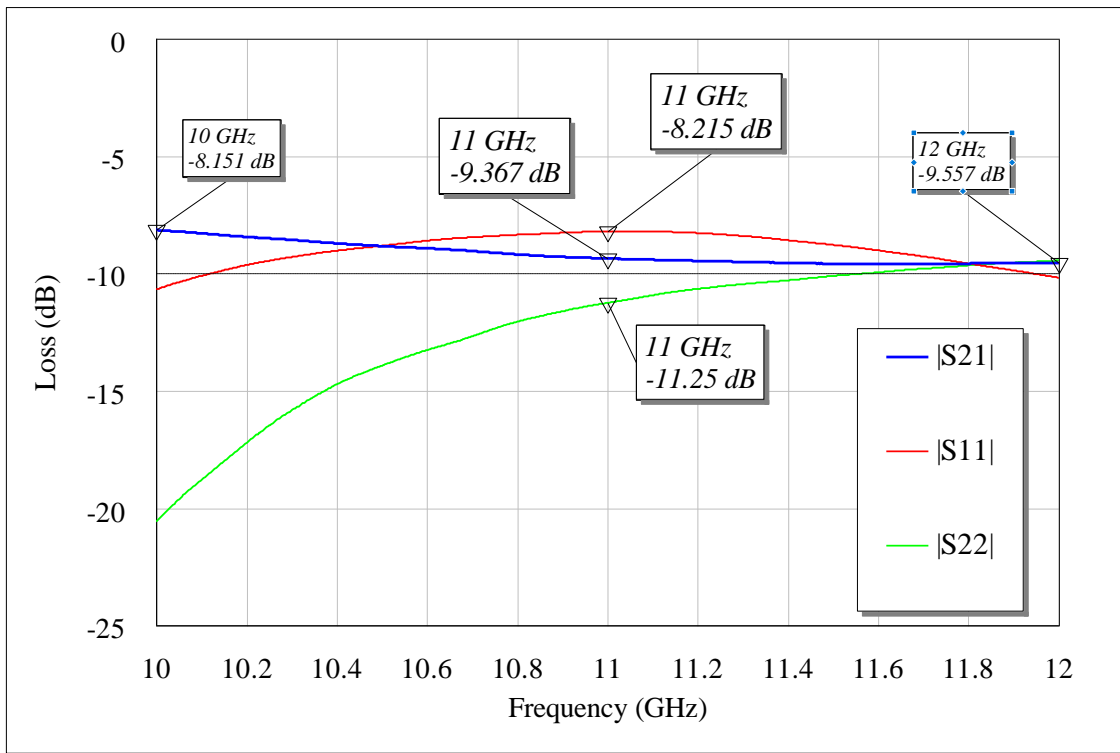


Figure 23. Measured S-parameters of the attenuator.

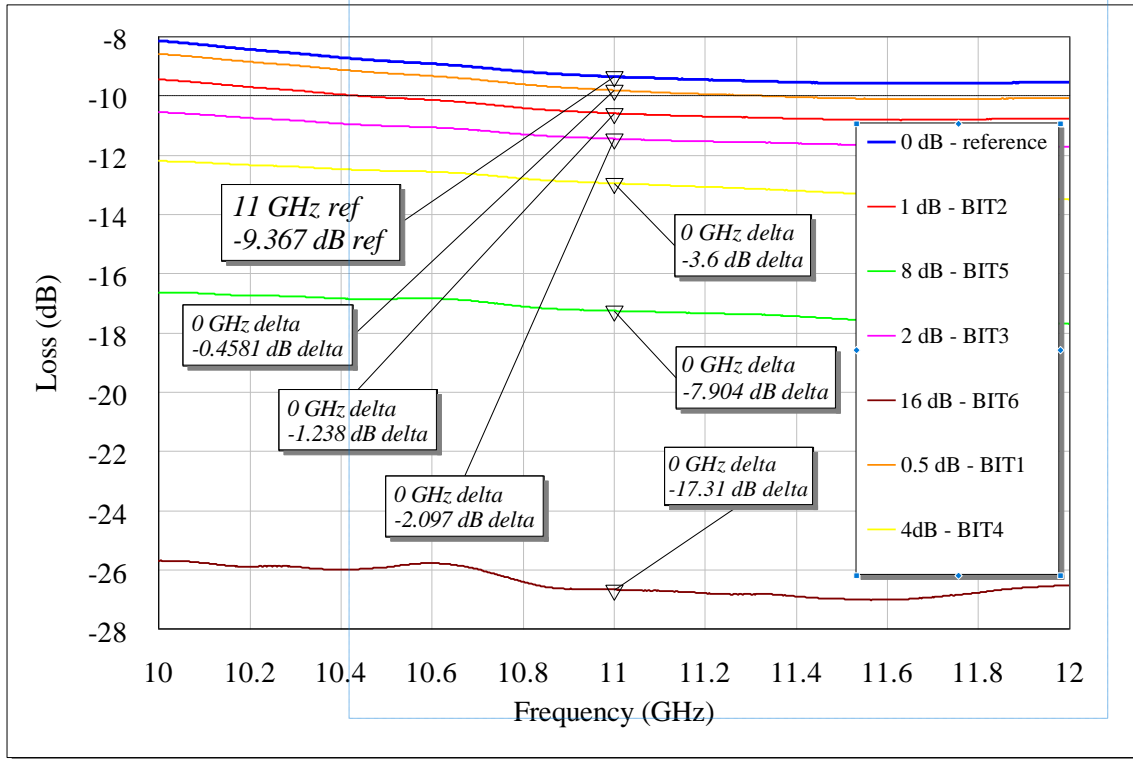


Fig. 24. Insertion loss for each significant bit.

From Fig. 22 we can conclude that insertion loss of designed phase shifter is ranging from 6.5 dB to 9 dB what is approximately 1.5-2 dB less than the same parameter according to datasheet for given frequency range. Input and output return loss for 11 GHz are below -10 dB which means that device is well matched at input and output.

Results on Fig. 23 show that the attenuator is well matched at the output for 11 GHz but not so well matched at the input. Insertion loss is approximately 2.5 dB less than corresponding datasheet parameter. Also Fig. 24 shows attenuation towards reference value for each significant bit set to logic „high“ state.

5.2. Microcontroller signal measurements

In order to ensure that application software for phase shifter is working correct and microcontroller sends the right in time domain signals which correspond to the given mode, the voltage at the output of microcontroller pin PB0 was measured with Keysight MSO-X 3034T oscilloscope (Fig. 25 and Fig. 26). Recall that pin PB0 serves to control LSB of phase shifter MMIC and, therefore, has the highest switch rate between logic states.

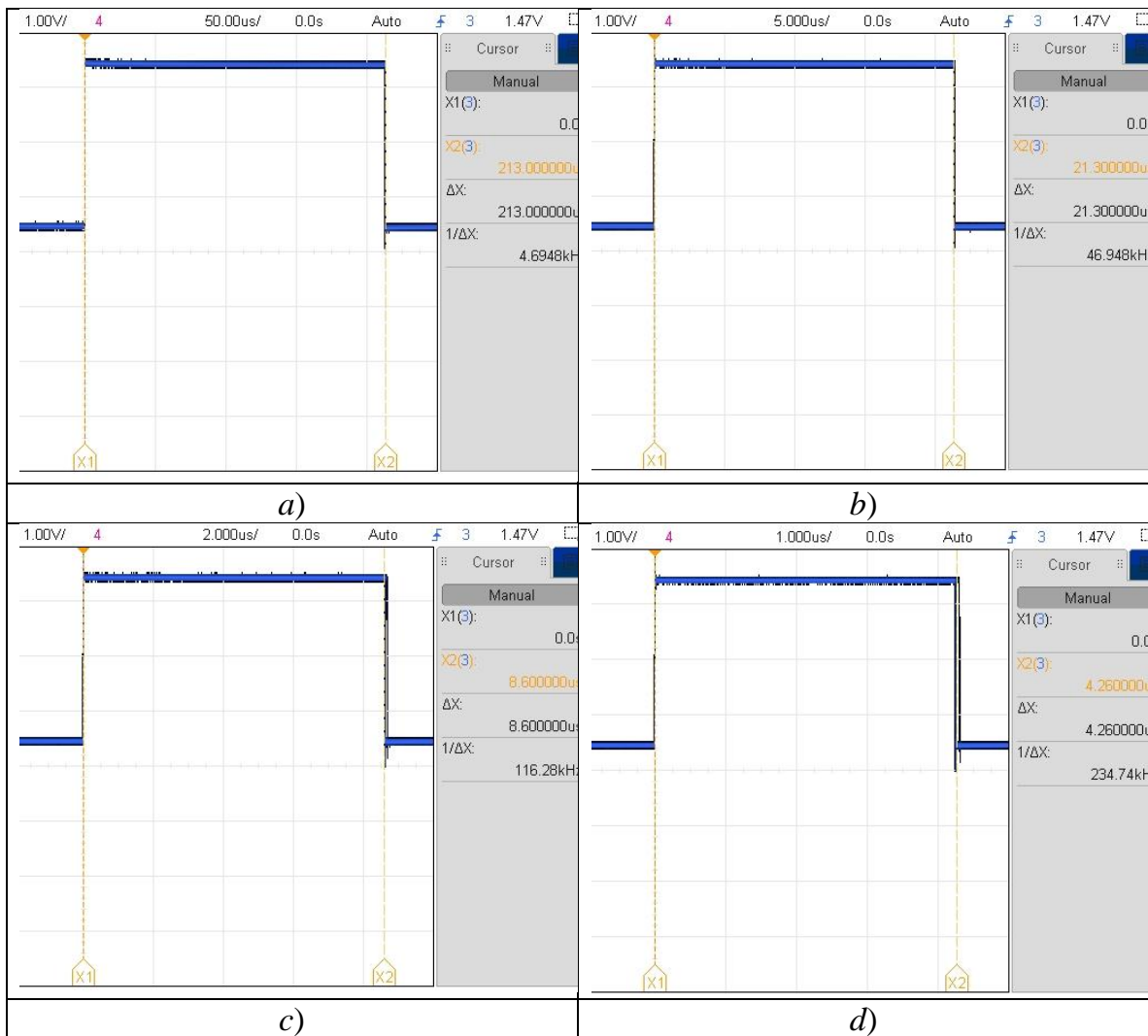


Fig. 25. Oscilloscope screenshots for: a) mode #1; b) mode #2; c) mode #3; d) mode #4.

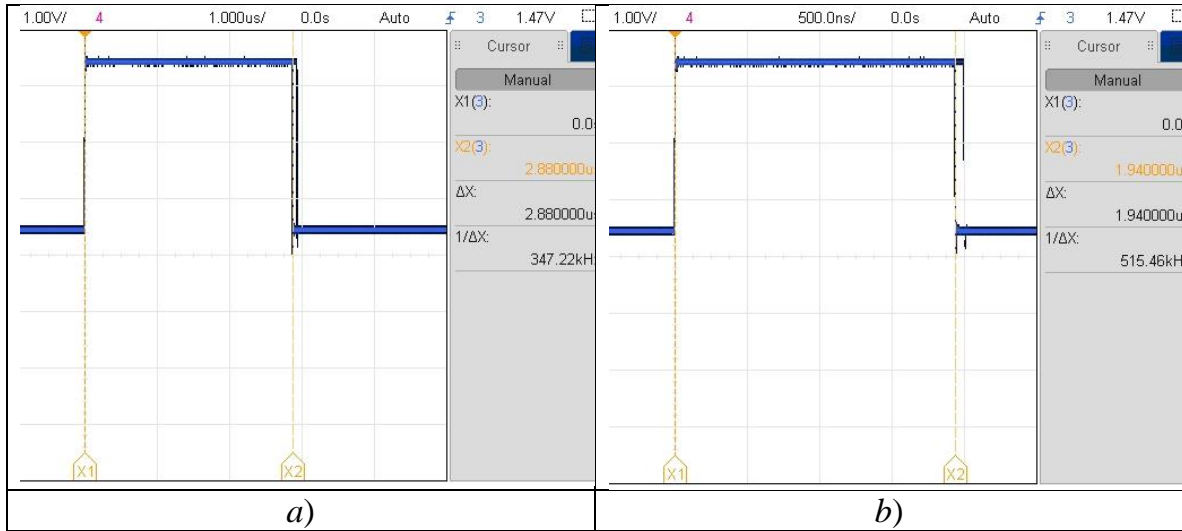
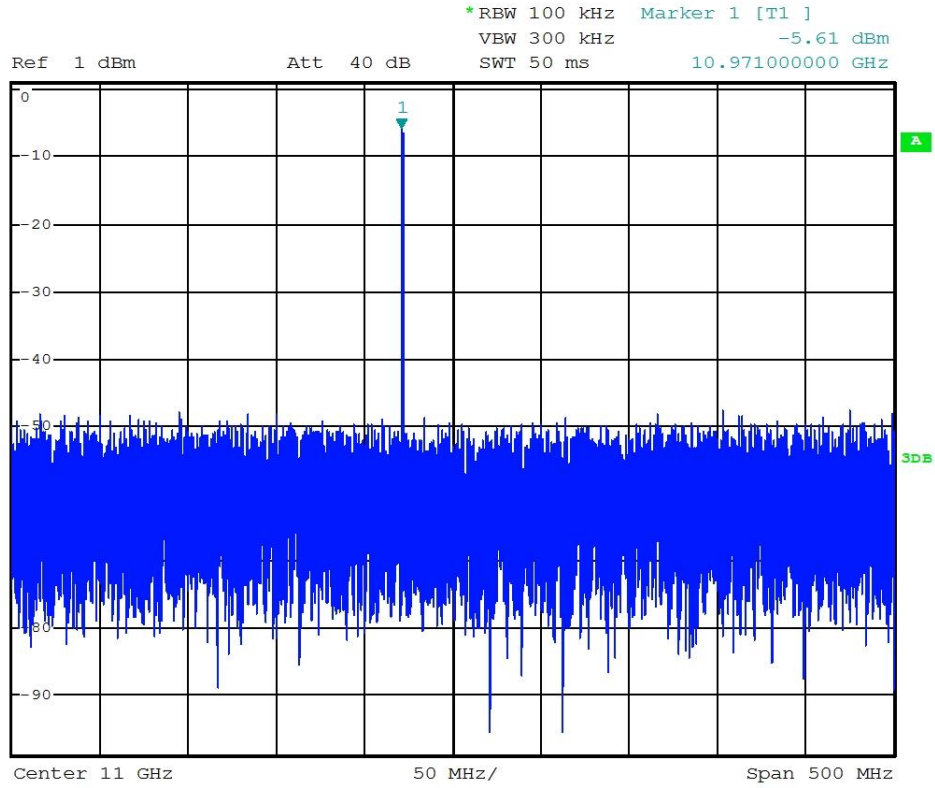


Fig. 26. Oscilloscope screenshots for: a) mode #5; b) mode #6.

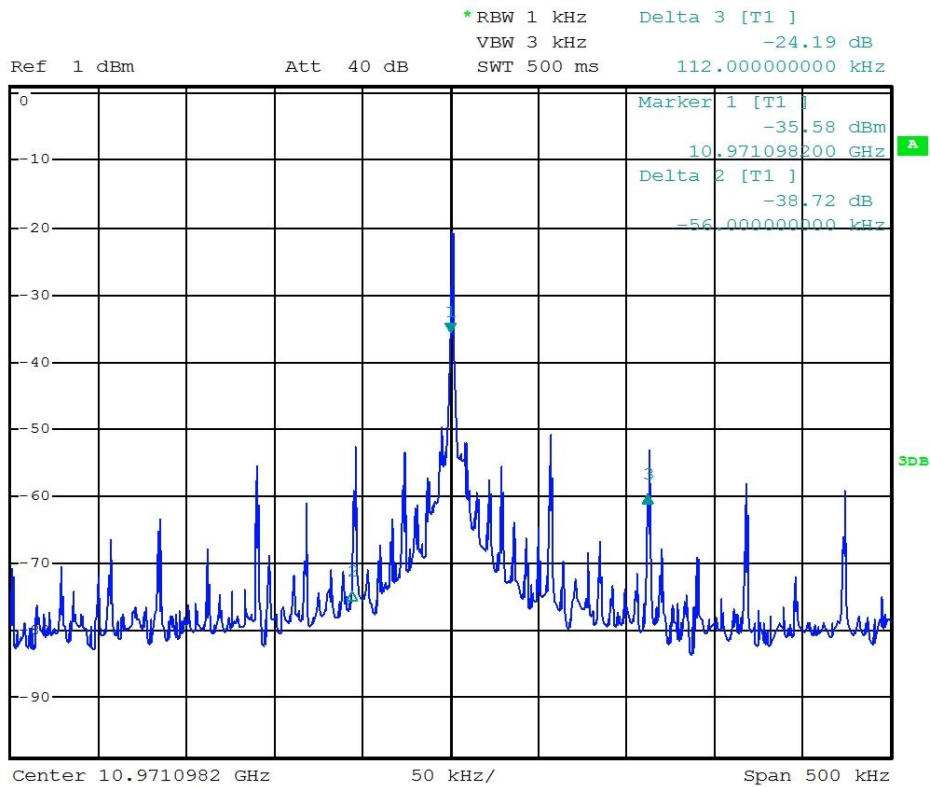
5.3. Signal spectrum measurement

This measurement was done to compare the RF signal generating by CW radar, and going directly through 20 dB attenuator to the phase shifter, with the RF signal at the output of the phase shifter. The measurement was performed using a Rohde&Schwarz spectral analyzer with a phase shifter set in a mode #5 with a maximum rate of phase change.

It can be seen from the Fig. 27 that the signal at the output of the phase shifter, as expected, has some parasitic phase modulation. The strongest side harmonic is located in 56 kilohertz from the main harmonica and 30 decibels below. It can be concluded that this signal is quite qualitative and these side harsonics will be filtered out during further processing in CW radar.



a)



b)

Fig. 27. Spectrum at: a) phase shifter input; b) phase shifter output.

5.4. Calibrator testing

The most important test was performed with setup shown on Fig 28. For simplicity of testing, calibrator was connected directly to 11 GHz CW radar by RF cables. In order to avoid amplifier in radar Rx chain to be overdriven, a 20 dB attenuator was used between Tx antenna output and input of phase shifter and also 15 dB attenuation of attenuator was set. Advanced Lecroy WaveRunner 640Zi oscilloscope was used to measure baseband signal at output of HP/LP filter and for data acquiring and saving. Phase shifter speed was set to simulate target radial velocities: 25 m/s, 50 m/s, 75 m/s and 110 m/s. 1 sec long signals were sampled at 10 MHz sampling rate and saved as DAT file format. Further data processing was done in Matlab.

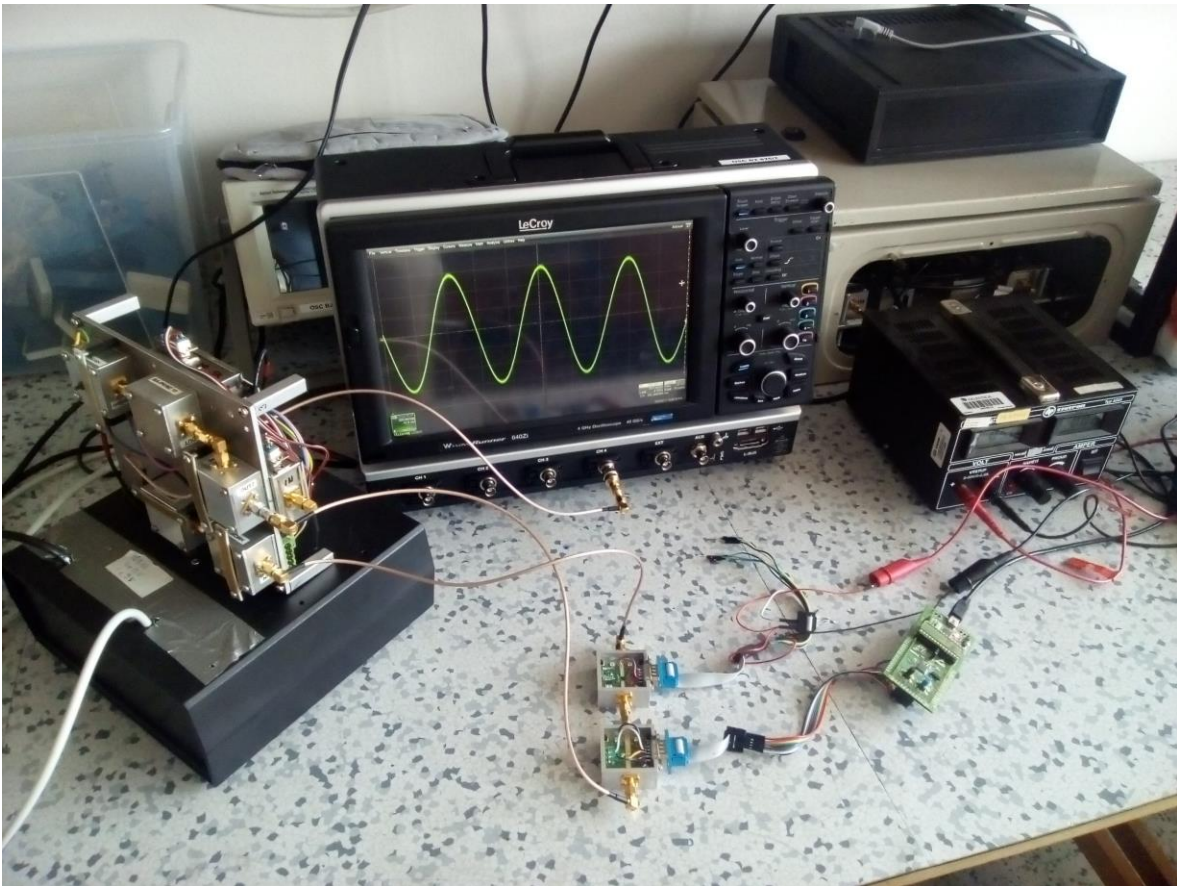


Fig. 28. Calibrator testing setup.

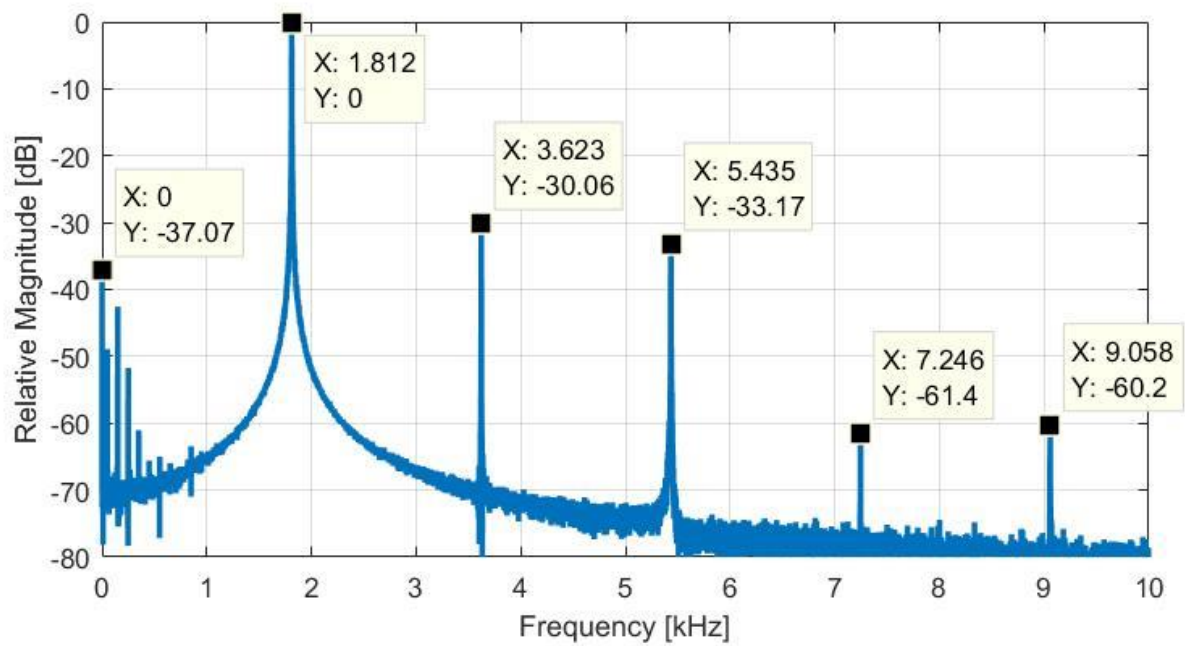
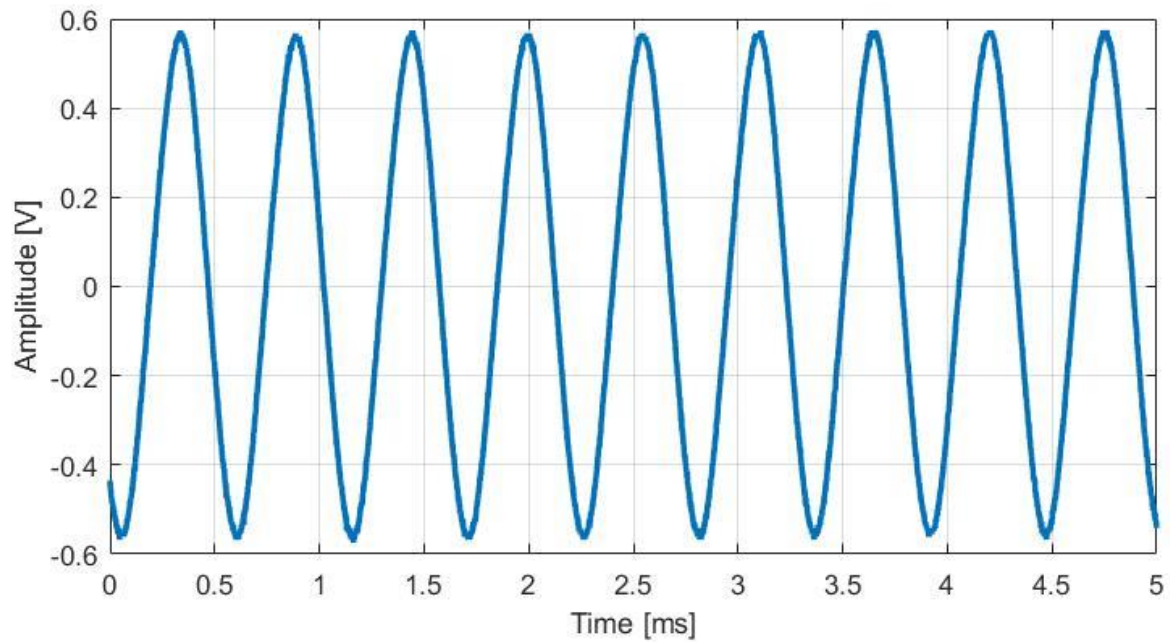


Fig. 29. Time domain waveform and corresponding FFT spectrum for simulating target with 25 m/s radial velocity.

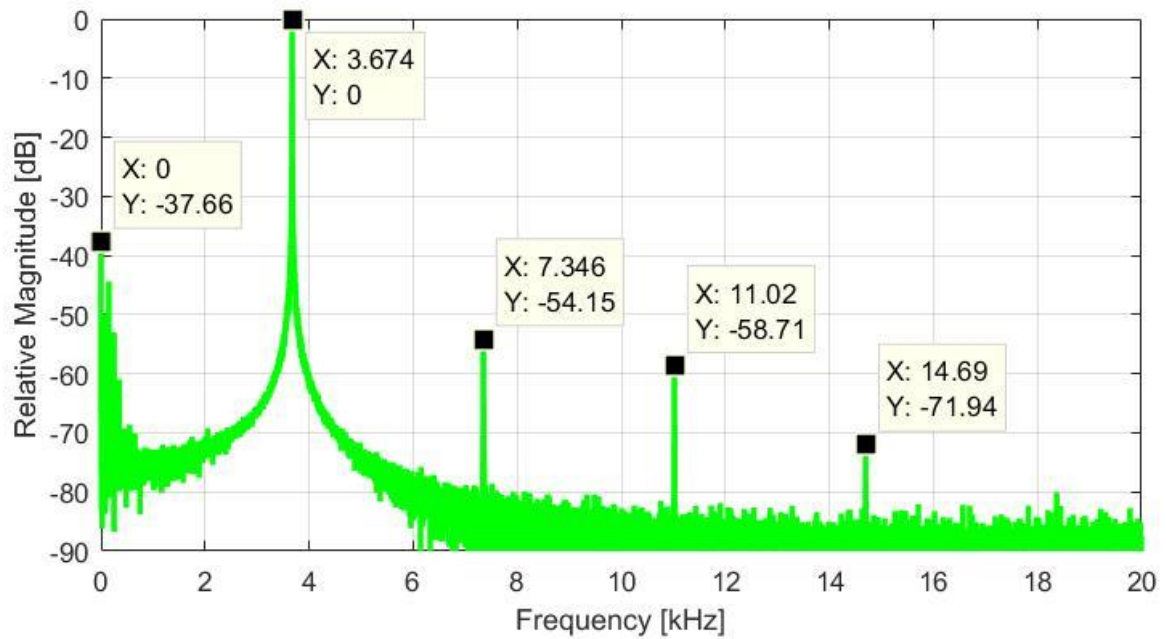
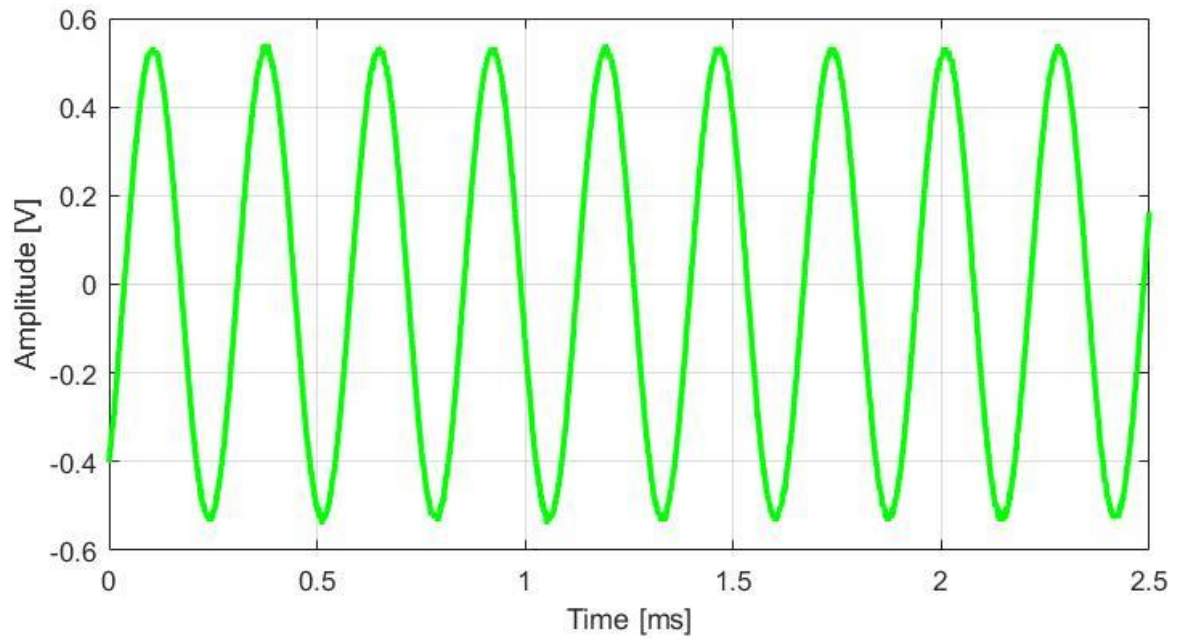


Fig. 30. Time domain waveform and corresponding FFT spectrum for simulating target with 50 m/s radial velocity.

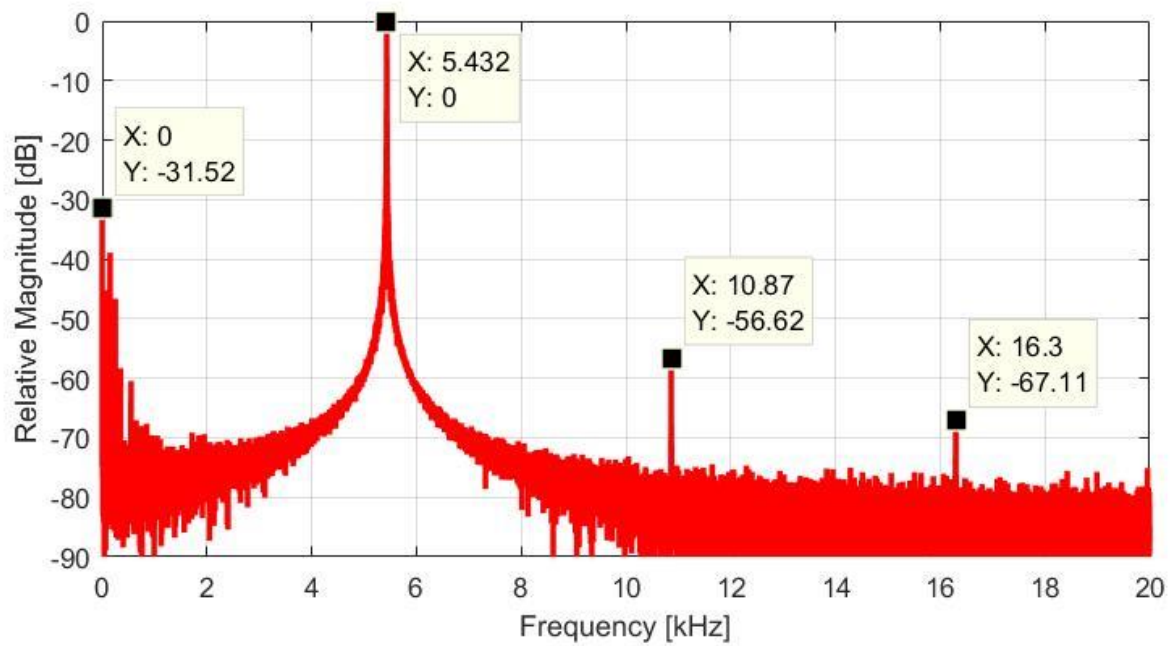
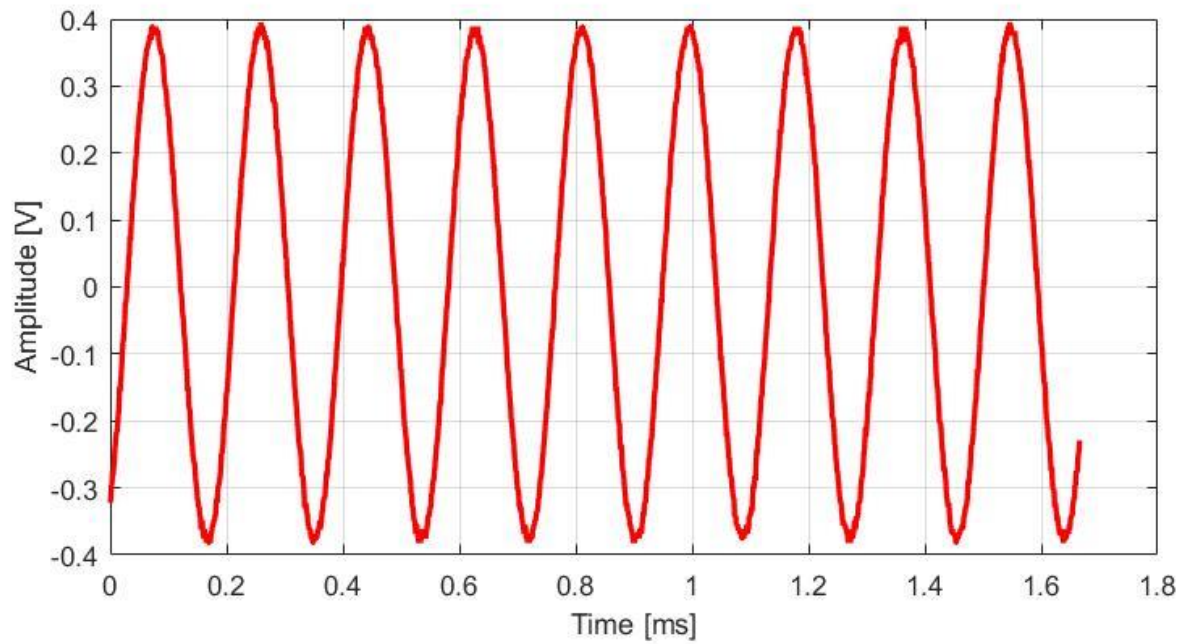


Fig. 31. Time domain waveform and corresponding FFT spectrum for simulating target with 75 m/s radial velocity.

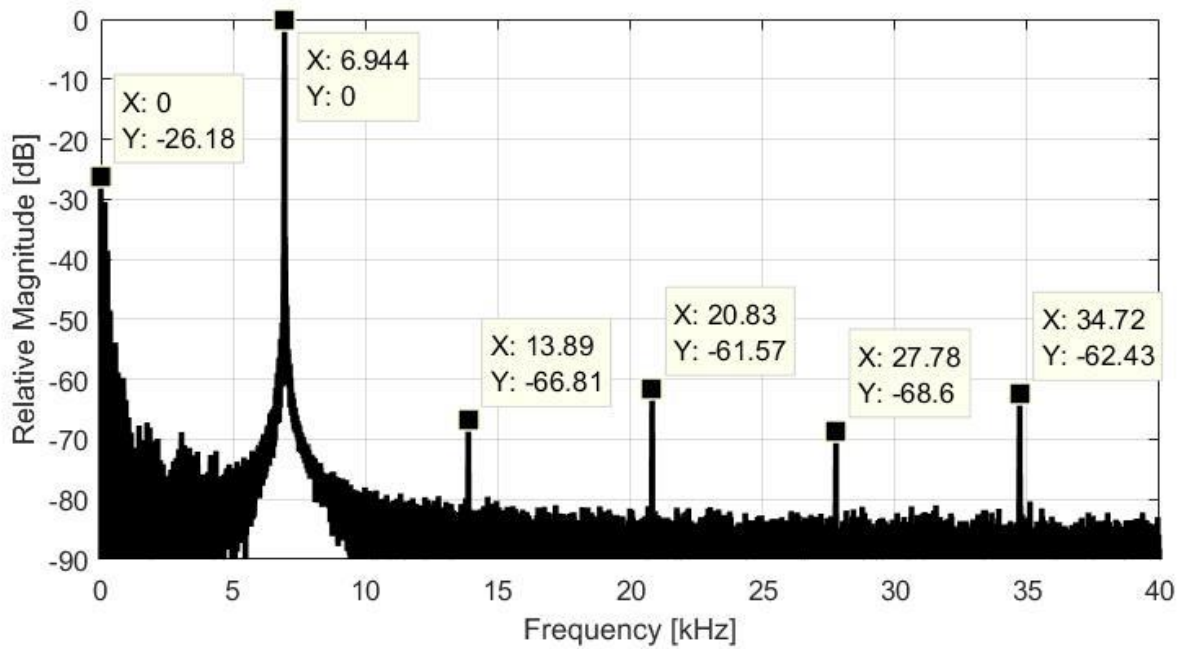
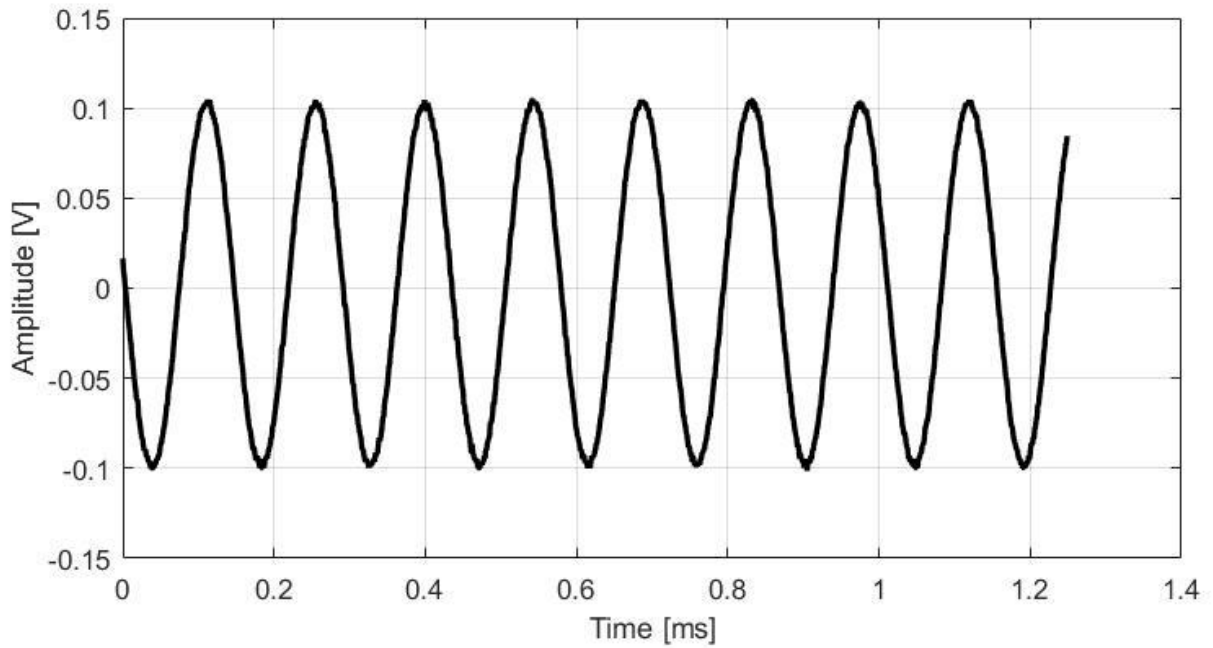


Fig. 32. Time domain waveform and corresponding FFT spectrum for simulating target with 110 m/s radial velocity.

From these graphs (Fig. 29 – Fig. 31), we can see that the processed signal at the output of the radar HP/LP filter has an almost pure harmonic waveform with a strong component at expected frequencies. The spectrum is stable and the simulated target velocity is constant and well defined.. Also, due to parasitic phase modulation and non-linearity in the Rx chain of the radar, signals contains the higher f_D harmonics which level at least 30 dB less in the case of simulating the target radial velocity of 25 m/s and this level decreases as the simulated velocity is increased. Evidently, filtering is affected these harmonics as, for example, amplitude of received signal is greatly reduced for last case with $f_D = 6.944$ kHz (Fig. 32).

Based on the measured and expected pseudo-Doppler shifts we can calculate the absolute error between them (see Table. 6) as:

$$Error = \frac{|Expected f_D - Resulted f_D|}{Expected f_D} \cdot 100\% \quad (10)$$

Table 6. Error of pseudo-Doppler frequency.

Simulated v_r , m/s	Expected f_D , kHz	Resulted f_D , kHz	Error, %
25	1.85	1.812	2
50	3.7	3.674	0.7
75	5.55	5.432	2.13
110	8.125	6.944	14.5

It could be seen from this table that within the limits of simulated velocity from 25 m/s to 75 m/s, the error is approximately 2% from expected value, which could be considered as quite good result. However, in case of maximum velocity of 110 m/s this error is quite significant - 14%. This behavior is most likely due to the behavior of the phase shifter at high phase-switching rates, but, unfortunately, there's no any transient measurements in the datasheet regarding the phase shifter response time to changes of the control signal.

To determine the maximum range of applicability of the calibrator with affordable accuracy, additional measurements should be made with a smaller step between simulating f_D .

Conclusions

This diploma thesis is concerned with designing, practical realization and experimental verification of a calibrator setup for testing 11 GHz band xCW radars. The setup, itself, consist of the digital controlled MMIC phase shifter, key element, the digital controlled MMIC attenuator and microcontroller to drive phase shifter.

Experimental testing of CW radar shows, that the setup is able to simulate moving target with radial velocity from 1 m/s up to 75 m/s with about 2% accuracy, generating quite pure stable sinusoidal signal at radar HP/LP filter output with almost negligible f_D -multiple side harmonics (the second one at least 30 dB less).

Realized setup may serve as a good basis for the following-up efforts focused on testing more complicated types of xCW radars (FMCW, PNCW, etc.) operating at 8-12 GHz frequency band or optimization calibrator setup using more advanced microcontroller. One may add, that realized phase shifter and attenuator, itself, also could be used in another application.

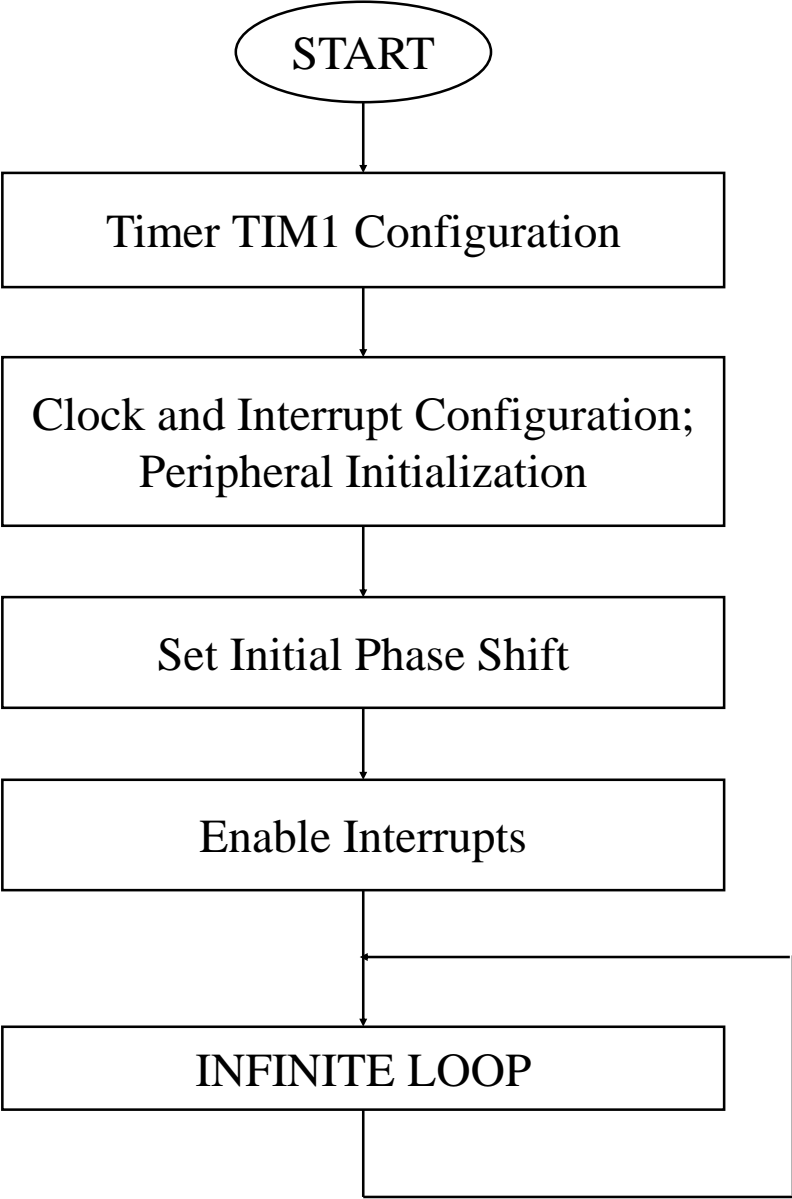
References

1. Griffiths H. D.: “New ideas in FM radar”, Electronics & Communication Engineering Journal, Volume: 2, Issue: 5, pp. 185-194, October 1990;
2. Hudec P., Raboch J., Randus M., Hoffmann K., Holub A., Svanda M., Polivka M.: “Microwave Radar Sensors for Active Defense Systems”, Proceedings of the EuRAD conference, Rome 2009;
3. Stove, A.G.: “Linear FMCW radar techniques”, IEE proceedings, vol. 139, no.5, pp. 343-350, 1992;
4. Plhák Zdeněk, “Kalibrátor dopplerovských radarů”, Diploma thesis, FEL CVUT, 2013;
5. <http://www.analog.com/media/en/technical-documentation/data-sheets/hmc642a.pdf>
6. <http://www.qorvo.com/products/d/da005089>
7. <https://cdn.macom.com/datasheets/MAPS-010166.pdf>
8. <http://www.analog.com/media/en/technical-documentation/data-sheets/hmc1018a.pdf>
9. <http://www.qorvo.com/products/d/da005017>
10. <https://cdn.macom.com/datasheets/MAAD-011021.pdf>
11. <http://www.mouser.com/ds/2/256/MAX850-MAX853-107740.pdf>
12. http://www.mouser.com/ds/2/447/PYu-RC0402_51_RoHS_L_6_r-8721.pdf
13. <http://www.mouser.com/ds/2/427/t58-748566.pdf>
14. http://www.pragoboard.cz/o_firme
15. <https://www.rogerscorp.com/documents/726/acs/RO4000-LaminatesData-sheet.pdf>
16. <http://www.jyebao.com.tw/product/detail/id/8754.html>

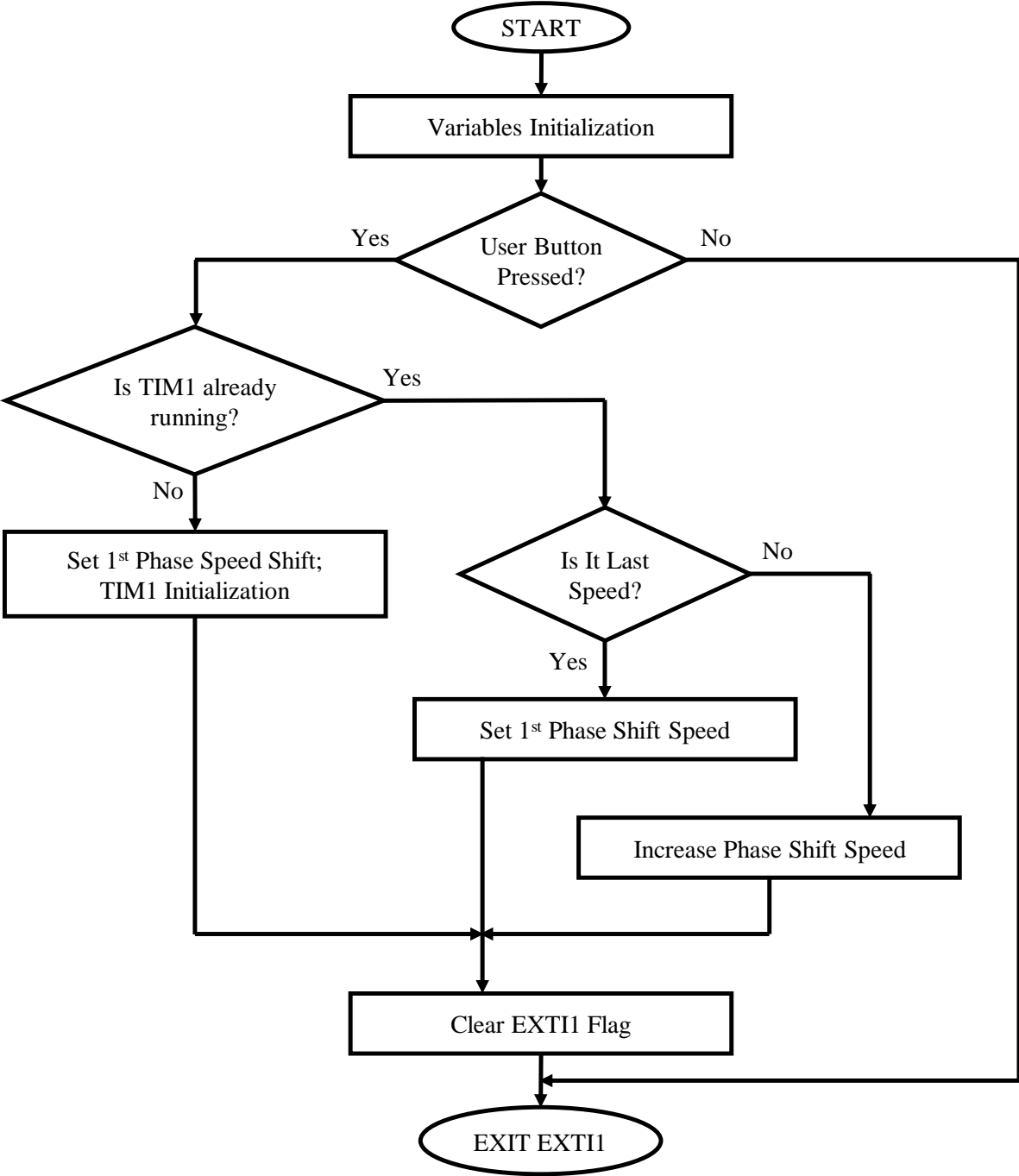
17. http://www.st.com/resource/en/user_manual/cd00278045.pdf
18. http://www.st.com/content/ccc/resource/technical/document/reference_manual/2e/3b/8c/8f/60/af/4b/2c/CD00218714.pdf/files/CD00218714.pdf/jcr:content/translations/en.CD00218714.pdf

Appendix A. Application Software Flowcharts

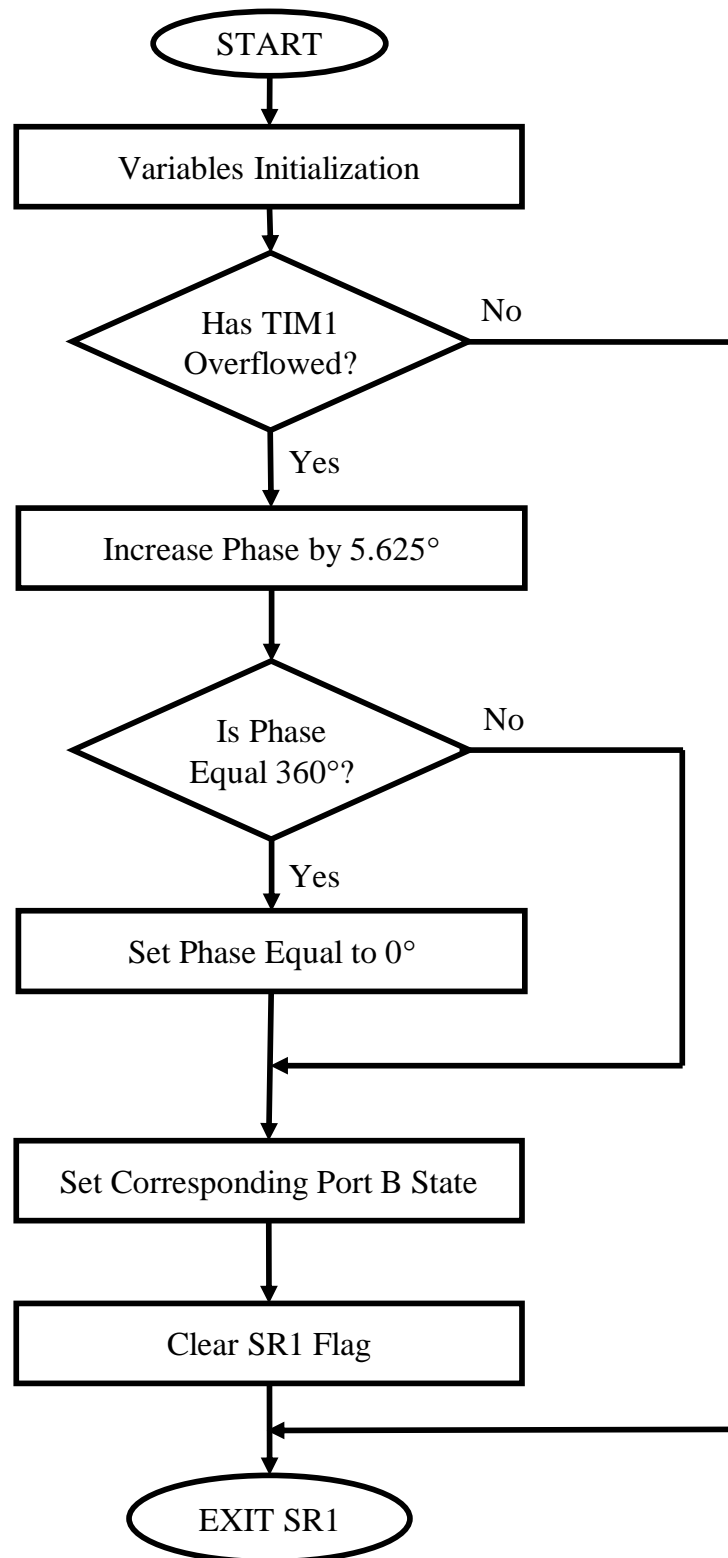
A.1. Main application flowchart



A.2. "User button pressed" interrupt flowchart



A.3. "TIM1 overflow" interrupt flowchart



Appendix B. Application Source Code Listing

B.1. Main program – *main.c*

```
/**
*****
*****
* @file    Diploma/main.c
* @author  Andrey Zidkov
* @version V2
* @date    05/2010
* @brief   Main program body
*****
*****

/* Includes -----
-----*/
#include "stm8l15x.h"
#include "stm8l15x_clk.h"

/* Main Program -----
-----*/
void main(void)
{
    // Set System Clock divider to 1
    CLK->CKDIVR = 0x00;

    /******* TIM1 Config *****/
    // Apply Internal Clock to TIM1
    CLK->PCKENR2 = 0x02;
    // Set Auto-Reload Register
    TIM1->ARRH = 0xFF;
    TIM1->ARRL = 0xFF;
    // Set Prescaler Register to 1
    TIM1->PSCRH = 0x00;
    TIM1->PSCRL = 0x01;
    // Enable interrupt
    TIM1->IER = 0x01;
    TIM1->EGR = 0x01;
    // Update request source
    TIM1->CR1 = 0x04;

    /******* Init Board key button and led *****/

```

```

// Interrupt sensitivity set to falling edge only for PC1
EXTI->CR1 = 0x0A;
// Init GPIO Port B
GPIOB->DDR |= 0x3F;
GPIOB->CR1 |= 0x3F;
GPIOB->CR2 |= 0x3F;
// Set initial 0deg phase shift
GPIOB->ODR = 60;
// Init GPIO Port C
GPIOC->DDR &= 0xFD;
GPIOC->CR1 &= 0xFD;
GPIOC->CR2 |= 0x02;
// Init GPIO Port E
GPIOE->DDR |= 0x80;
GPIOE->CR1 |= 0x80;
GPIOE->CR2 |= 0x80;
// Light on green LED
GPIOE->ODR |= 0x80;

// Enable Interrupts
enableInterrupts();

/* Infinite loop */
while (1)
{
    //
}
}

```

B.2. Interrupt routine – *stm8l15x_it.c*

```
/**
*****
*****
* @file    Diploma/stm8l15x_it.c
* @author  Andrey Zidkov
* @version V2
* @date    05/2010
* @brief   Main Interrupt Service Routines.

/* Includes -----
-----*/
#include "stm8l15x_it.h"

/* Private variables -----
-----*/
__CONST uint8_t PhaseTable[64] = {60, 61, 62, 63, 56, 57, 58,
59,
                                     52, 53, 54, 55, 48, 49, 50, 51,
                                     44, 45, 46, 47, 40, 41, 42, 43,
                                     36, 37, 38, 39, 32, 33, 34, 35,
                                     28, 29, 30, 31, 24, 25, 26, 27,
                                     20, 21, 22, 23, 16, 17, 18, 19,
                                     12, 13, 14, 15, 8, 9, 10, 11,
                                     4, 5, 6, 7, 0, 1, 2, 3};
uint8_t phase_state = 0;
__CONST uint8_t SpeedTableH[6] = { 6, 0, 0, 0,
0, 0};
__CONST uint8_t SpeedTableL[6] = {169, 170, 68, 33, 22, 17};
uint8_t speed = 6;

...

...

/**
* @brief External IT PIN1 Interrupt routine.
```

```

*   On User button pressed:
*   Set corresponding Auto-Reload Register Value
*/
INTERRUPT_HANDLER(EXTI1_IRQHandler, 9)
{
    // IT Linked to USER button present on board on PC1
    detected on falling edge only
    if (!(GPIOC->IDR & 0x02))
    {
        // Check if TIM1 already running
        if (!(TIM1->CR1 & 0x01))
        {
            // Set phase shift speed
            speed = 0;

            // Set corresponding Auto-Reload Register Value
            TIM1->ARRH = SpeedTableH[speed];
            TIM1->ARRL = SpeedTableL[speed];

            // Enable Timer TIM1
            TIM1->CR1 = 0x01;
        }
        else
        {
            speed++;
            if (speed>5)
                speed = 0;

            // Set corresponding Auto-Reload Register Value
            TIM1->ARRH = SpeedTableH[speed];
            TIM1->ARRL = SpeedTableL[speed];

            // Light on/off green LED
            GPIOE->ODR ^= 0x80;
        }
    }

    // Clear interrupt flag
    EXTI->SR1 = (uint8_t)0x22;
}

...

...

```

```

/**
 * @brief TIM1 Update/Overflow/Trigger/Commutation Interrupt
routine
 *   At TIM1 Overflow:
 *   Increase phase by one LSB (5.625 degree)
 */
INTERRUPT_HANDLER(TIM1_UPD_OVF_TRG_COM_IRQHandler, 23)
{

    if (TIM1->SR1 & 0x01)
    {
        // Increase phase by 5.625 degree
        phase_state++;
        if (phase_state > 63)
            phase_state = 0;

        // Set corresponding output state
        GPIOB->ODR = PhaseTable[phase_state];
    }

    // Clear interrupt flag
    TIM1->SR1 = 0x00;
}

...

```